

Review

A Comprehensive Understanding of Thermal Barrier Coatings (TBCs): Applications, Materials, Coating Design and Failure Mechanisms

Maria Bogdan and Ildiko Peter * 

Department of Industrial Engineering and Management, Faculty of Engineering and Information Technology, George Emil Palade University of Medicine, Pharmacy, Science and Technology of Târgu Mureș, 540142 Târgu Mureș, Romania; maria.bogdan@umfst.ro

* Correspondence: ildiko.peter@umfst.ro

Abstract: This review offers a comprehensive analysis of thermal barrier coatings (TBCs) applied to metallic materials. By reviewing the recent literature, this paper reports on a collection of technical information, involving the structure and role of TBCs, various materials and coating processes, as well as the mechanisms involved in the durability and failure of TBCs. Although TBCs have been successfully utilized in advanced applications for nearly five decades, they continue to be a subject of keen interest and ongoing study in the world of materials science, with overviews of the field's evolution remaining ever relevant. Thus, this paper outlines the current requirements of the main application areas of TBCs (aerospace, power generation and the automotive and naval industries) and the properties and resistance to thermal, mechanical and chemical stress of the different types of materials used, such as zirconates, niobates, tantalates or mullite. Additionally, recent approaches in the literature, such as high-entropy coatings and multilayer coatings, are presented and discussed. By analyzing the failure processes of TBCs, issues related to delamination, spallation, erosion and oxidation are revealed. Integrating TBCs with the latest generations of superalloys, as well as examining heat transfer mechanisms, could represent key areas for in-depth study.

Keywords: thermal barrier coatings (TBCs); yttria-stabilized zirconia (YSZ); coating techniques; multi-layered coatings; porosity; thermal expansion; failure mechanisms



Citation: Bogdan, M.; Peter, I. A. Comprehensive Understanding of Thermal Barrier Coatings (TBCs): Applications, Materials, Coating Design and Failure Mechanisms. *Metals* **2024**, *14*, 575. <https://doi.org/10.3390/met14050575>

Academic Editor: Liang-Yu Chen

Received: 3 April 2024

Revised: 2 May 2024

Accepted: 3 May 2024

Published: 13 May 2024



Copyright: © 2024 by the authors. Licensee MDPI, Basel, Switzerland. This article is an open access article distributed under the terms and conditions of the Creative Commons Attribution (CC BY) license (<https://creativecommons.org/licenses/by/4.0/>).

1. Introduction

In this review paper, a general overview of the current landscape related to TBCs is provided. It is important to note that this review paper does not intend to fully cover all aspects of the topic. Instead, it aims to present and discuss some crucial details within this extensive field, highlighting the challenges and opportunities in the development of thermal protective coatings across a variety of structural and compositional aspects. The information presented is drawn from literature data and includes observations and individual insights on this increasingly relevant topic in advanced industries.

With the initial research on TBCs beginning in an incipient stage in the late 1940s, within the aeronautics field, evolution has persisted with each passing decade, reaching a pivotal period in the 1970s. During this time, a comprehensive material-processing method was developed (zirconia–yttria coatings/plasma-spray technique), which remains relevant to this day. Progress continued into the 1980s and 1990s with the advancement of computer-simulated testing and the evolution of superalloy substrates, culminating in the present day with nanotechnologies and superior combinations of elements capable of meeting the demands of a wide range of applications.

Special industries such as the aerospace, automotive and energy production industries and even the maritime field share not only high manufacturing standards, including the need for precision engineering and accurate quality control, but also the challenge of operating

in incredibly harsh environments. Although these advanced fields utilize materials with good characteristics to ensure resistance to harmful environmental factors, these materials can reach their performance peak, hindering the systems' overall potential [1]. Additional aspects related to evolution and application domains will be discussed in detail in the sections below.

TBCs represent a revolutionary innovation in materials engineering, defining a multi-layered system, typically containing an outer ceramic layer placed over a metallic bonding layer, which jointly serves to isolate the component's material from the external environment and to reduce the impacts exerted by it. Not only are they essential for sustainability by extending the lifespan and usage time of systems by protecting components from the adverse effects of high temperatures, large temperature variations, corrosion and oxidation but they also contribute to enhancing the performance of various equipment through isolation of the working environment [2,3].

2. Brief History of TBCs' Evolution over Time

Access to different materials, techniques and experimental information over time has had a significant impact on how the development of approaches for TBCs has evolved. The great journey of materials research and methods can be traced back to the history of TBCs, from the earliest attempts to protect components at severe temperatures to the most sophisticated solutions available nowadays. This path includes several stages of development, impacted by developments in science and technology and the constantly shifting demands of this industrial area. The following image (Figure 1) schematically illustrates the main stages of TBCs' evolution and the elements involved in their development.

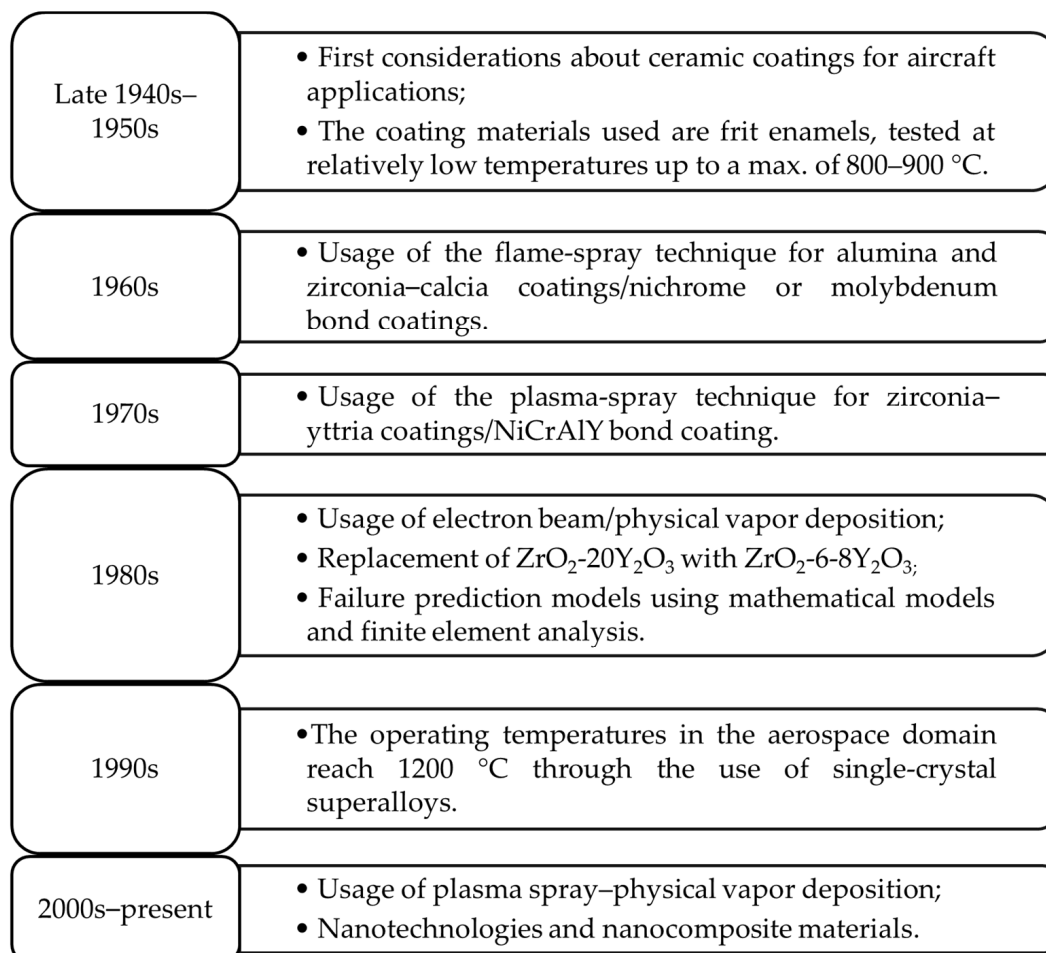


Figure 1. Timeline of TBCs development (data from Refs. [4–11]).

Following an analysis of the specialized literature, the first publication regarding ceramic coatings dates back to 1947, performed by Harrison and Moore at the National Advisory Committee for Aeronautics, Washington, DC, USA where they analyzed ceramic refractory mixtures including alumina, chromium oxide and cobalt with the intention of using them to protect turbine blades [4].

The year 1976 stands as a significant milestone, indicating the dawn of the modern era of TBCs. This moment was marked by the successful testing of the feasibility of a ZrO_2 - $12Y_2O_3$ /NiCrAlY coating on J-75 turbine blades. This study set the direction for TBC research, establishing yttria-stabilized zirconia (YSZ) as the reference material for coatings and outlining a coating structure consisting of only two layers: the topcoat and the bond coat [7,8].

Current directions in TBC development involve the development of new compositions aimed at reducing phonon and photon transport, nano-structural approaches, as well as the employment of multi-layer and functionally graded coatings. The focus is also on developing new processing technologies and optimizing existing methods and parameters for their fabrication to enable TBCs' use at higher temperatures [12,13].

3. The Main Application Areas of TBCs

To highlight the origin of importance, the necessity for evolution and the requirements that TBCs must meet, a description of the principal areas of application is necessary. For a better understanding, this part will be divided into multiple sections, thereby highlighting the various applications of TBCs. Figure 2 illustrates the main application domains of TBCs.



a. Aerospace applications

- Commonly used for gas turbines and rocket engines;
- Extreme temperature variations and exposure to constant temperatures of 1500 °C.



b. Power generation

- Continuously evolving field;
- The new applications reach temperatures of 1700 °C;
- Requirements for long-term use.



c. Automotive applications

- Commonly used for internal combustion engines;
- Demanding application due to knocking and increased NOx emissions.



d. Naval industry

- Used in propulsion systems, similar to applications in the power generation industry;
- Additional protection against corrosive environments.

Figure 2. The main application areas of TBCs.

3.1. Aerospace Applications

In the aerospace sector, TBCs are widely employed to safeguard components within the propulsion systems and auxiliary equipment of various aircraft types (military, civilian airplanes, etc.) as well as rockets [14].

During combustion, rocket engine combustion chambers are subjected to extreme heat, with gas temperatures reaching up to 3200 °C. To lower wall temperatures, a special copper cooling system is employed, through which liquid hydrogen at −240 °C is circulated. This significant temperature differential causes substantial thermal stress, increasing oxidation risk. TBCs are applied on the surface of exposed components to prevent damage and support temperature reduction [15,16]. The coatings must effectively withstand both low and high pressures (<1–10 MPa) and thermal shock from transitioning between high temperatures and cryogenic conditions [17].

In aircraft design, TBCs are crucial for shielding gas turbine components from damage caused by high combustion temperatures. The temperature on the surface of these components can intensify between 1300 °C and over 1500 °C for advanced turbine models, influenced by various operational parameters [3,10,18]. These temperatures approach or can even exceed the melting point of the alloys used in their manufacture (e.g., Hastelloy X-MP 1260–1355 °C; Rene 95-MP 1343 °C; IN 718-MP 1260–1336 °C, etc.) [19,20].

In turbines, heat transfer occurs through a combination of processes: convection and radiation, especially between the high-temperature exhaust gas flow and components, and through conduction within the components themselves as internal heat distribution. The reverse also applies to the system's cooling process [21].

Redesigning the configurations of the components, particularly those related to cooling mechanisms, can act as an approach to control overheating issues. Yet, this method is not always the easiest, least expensive or most effective option available [22,23].

Employing TBC alongside cooling mechanisms not only lowers temperatures and extends the lifespan of turbines but also enables higher combustion temperatures for increased efficiency output. By applying a coating with low thermal conductivity, the surface temperature can be reduced by up to 300 °C [24].

These general principles are also applicable to turbines designed for power generation.

Ali et al. [25] demonstrated in their study that increasing the thickness of TBCs from 100 µm to 500 µm results in a reduction in the surface temperature on a blade by 6.5% and decreases the coolant's temperature by 50 °C. In their simulation, they employed an Inconel-718 substrate with $\text{La}_2\text{Zr}_2\text{O}_7$ as the TBC material.

The specific literature does not provide a lot of precise information about the lifespan of TBCs in these systems, as it depends on many factors that cannot be accurately estimated. However, as a general guideline, a lifespan of about 1000 h can usually be considered for jet engines undergoing multiple cycles of heating to the mentioned temperatures and cooling to ambient temperature [10]. After reaching the maximum allowable deterioration, the TBC is replaced [26].

3.2. Power Generation

Even though there are many possibilities for energy generation nowadays, turbines are still used for their efficiency, flexibility, compatibility with various fuels, durability and scalability [27,28]. For example, it is expected that natural gas will become the main fuel source for power generation by the year 2035 [29]. Following international reports, between 2020 and 2029, it is expected that, globally, there will be more than 4200 turbines sold, amounting to a total value of over USD 102 billion [30]. In this anticipated context, turbine manufacturers will be required to respond to market demand, not only in a quantitative manner but also by focusing on improving the efficiency and performance of the turbines produced. Enhancing turbine efficiency, with rotor inlet temperatures exceeding 1700 °C and over 1000 °C on blades, necessitates the use of high-performance TBCs [31].

Most studies discuss virtual simulations of coating effects. In their study, Pirin et al. [32] simulate the effect of coatings with 8YSZ, Mg_2SiO_4 , $\text{Y}_3\text{Ce}_7\text{Ta}_2\text{O}_{23.5}$ and $\text{Yb}_3\text{Ce}_7\text{Ta}_2\text{O}_{23.5}$ on the

blade and nozzle 3D models of a micro gas turbine. The most significant stress reduction in the substrate is observed with Mg_2SiO_4 , exceeding 40 MPa for the nozzle and over 20 MPa for the blade. Additionally, in the hotspots, a temperature decrease of nearly 80 °C is noted for the nozzle and over 10 °C for the blade, all in comparison with the uncoated elements.

Typically, turbines used in power generation are designed to last several decades, with their lifespan depending heavily on operating conditions, fuel use and maintenance. TBCs applied on the components of these turbines have to meet a lifespan of up to 30,000 h under oxidative and corrosive operating conditions at temperatures exceeding 1000 °C [33].

3.3. Automotive Applications

The automotive field employs TBCs, particularly in exhaust systems and internal combustion engines. During the combustion process inside the cylinders, the temperatures reached by the air–fuel mixture in gasoline engines can climb to approximately 2400 °C. In contrast, diesel engines experience even higher temperatures, reaching values of around 3000 °C [34,35]. Thus, the engine's internal components such as the valves, pistons and cylinder walls absorb a considerable amount of heat, despite being equipped with special cooling systems [35]. According to the Society of Automotive Engineers [36], surface temperatures within the combustion chamber of a spark ignition (SI) engine were observed to vary between 142 °C and 258 °C for conditions ranging from 1400 to 3200 RPM, indicating a significant fluctuation in thermal load with engine speed. Typically, the piston head reaches temperatures over 300 °C, while the exhaust valve's temperature may surpass 700 °C [35].

To protect the engine's combustion chamber against premature deterioration caused by high temperatures and compounds present in the fuel, ceramic TBC coatings are applied, providing protection against thermal and chemical corrosion and oxidation. Additionally, TBCs aid in reducing environmental pollution caused by the burning of fuels in diesel, petrol or biofuel engines through insulation of the combustion chamber. This technology helps in minimizing heat losses, thereby facilitating more complete combustion. This approach can not only decrease harmful gas emissions (nitrogen oxide-NO, carbon monoxide-CO, hydrocarbons (HC), smoke, etc.) but also increase the engine's power and efficiency [37–39].

The thermal insulation capability effect was illustrated by Liu et al. [40], who reported in a simulation that applying a ceramic layer with a thickness of 370 µm to the top face of a piston results in a temperature decrease of over 50 °C in the throat of the piston.

According to the results of an experimental study by Das et al. [41] conducted on a diesel engine, it was found that a plasma-sprayed partially stabilized zirconia (PSZ) TBC applied to piston crowns of 250, 350 and 450 µm thicknesses can reduce fuel consumption by up to 10%, significantly decrease smoke emissions by nearly 50% and lower HC and CO emissions by up to 40%. However, NO_x emissions experienced an increase ranging from 7 to 11%.

Based on the research reported by Raghu et al. [42], it was demonstrated that coating a diesel engine's piston with Air plasma sprayed YSZ/NiFeCoCrAlY led to a 16% reduction in fuel consumption, a 7% increase in brake thermal efficiency and an improvement in mechanical efficiency of over 10%.

The experimental study conducted by Karthickeyan et al. [43] on a biodiesel engine, which involved altering the ratio of pumpkin seed oil and diesel, revealed that applying a 400 µm coating of plasma-sprayed PSZ/ Al_2TiO_5 on the piston crown, cylinder head and valves resulted in a notable increase in NO_x emissions, along with a reduction in HC and smoke when compared to a combustion chamber without a coating.

In some of the studies presented above [41,43], a contradictory behavior of emissions can be observed despite the benefits expected from the use of TBCs. Uchida [44] provides an overview of the effect of a TBC insulation applied to the components of the combustion chamber, highlighting that in diesel engines, it leads to increased emissions of NO_x and particulates, while in gasoline engines, it exacerbates the tendency to knock. These effects are due to the increase in temperature in the combustion chamber because the thermal insulation provided by the TBC limits too much dissipation of heat to the rest of the components. Durat et al. [45] highlight this through simulations conducted on a piston

partially covered with a TBC on the upper surface. The study shows a temperature increase at the coating level by up to 55% for Mg-PSZ and up to 30% for Y-PSZ, both compared to the uncovered piston. The smaller increase in the case of Y-PSZ is due to the higher thermal conductivity ($1.4 \text{ Wm}^{-1}\text{K}^{-1}$) that allows for greater heat diffusion compared to Mg-PSZ (thermal conductivity: $0.8 \text{ Wm}^{-1}\text{K}^{-1}$).

It is also known and has been experimentally proven that beyond a certain threshold, higher combustion temperatures lead to an increase in NO_x emissions, a phenomenon that also occurs in diesel engines [46,47].

In the case of SI engines, a high temperature in the combustion chamber leads to knock, a phenomenon characterized by the premature detonation of the air–fuel mixture before the spark plug ignites, which can cause severe damage [48].

Nevertheless, there exist technical strategies such as the rational selection of materials and the appropriate adaptation of the coating's thickness layer, alongside other technical approaches related to engine design and equipment, that integrate TBCs to enhance engine performance and mitigate or eliminate the previously mentioned adverse effects [48,49]. Additionally, this topic may serve as a promising avenue for future research.

3.4. Naval Industry

Even if the scientific literature is not yet complete with studies focusing on the specific application of TBCs in the marine sector, the potential of these technologies to enhance efficiency and extend the lifespan of marine propulsion systems has garnered special attention. The focal means of propulsion in the maritime domain include gas turbines, diesel engines and various hybrid systems [50,51].

The approach to implementing TBCs and the objectives followed are comparable to those in aerospace, energy production or the automotive industry, albeit scaled to the unique dimensions of marine applications. Additionally, TBCs offer the added benefit of acting as a protective barrier against the corrosive and humid conditions characteristic of the marine environment, thanks to the superior characteristics of the ceramic layer. TBCs can undergo testing in molten salt baths such as $\text{Na}_2\text{SO}_4 + \text{V}_2\text{O}_5$ [52] or $\text{Na}_2\text{SO}_4 + \text{NaCl}$ [53,54] to assess their resistance to extreme corrosive attack due to the marine environment and the fuels used.

4. Configuration of TBCs

In order to understand the mechanism behind TBCs and how they serve to offer corrosion, wear and thermal protection across various industrial applications, it is crucial to discuss their fundamental structure. These coatings are made up of multiple layers, each fulfilling a unique role in ensuring the durability and effectiveness of the TBC system.

These layered systems are made from several materials with different natures and chemical properties. Such a system is applied onto a base material (*substrate*) and conventionally contains a *bond coat* (BC) and a ceramic *topcoat* (TC). During thermal exposure, between these two layers, a third layer called *thermally grown oxide* (TGO) develops [55,56].

The configuration of a classic TBC structure is illustrated in Figure 3.

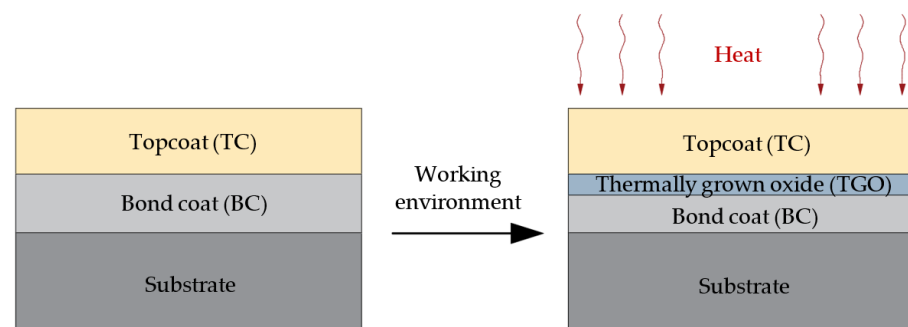


Figure 3. General TBC structure.

4.1. Substrate

The substrate represents the fundamental metallic component onto which the TBC is applied. Its main function is to provide structural support and allow the mechanical loads of the assembly. Its thickness is determined by the application requirements and component design. Due to their exceptional mechanical strength, corrosion resistance and high temperature resistance, superalloys are frequently used as substrates in a wide range of high-temperature applications [57].

Typically, the substrate materials in a TBC system are Ni- or Co-based superalloys, which initially included the classic polycrystalline form, followed by the single-crystal form with a higher melting point due to the lack of grain boundaries. The utilization of the single-crystal form in gas turbine engines dates back to 1995 [58]. Ni-/Co-based superalloys can contain up to 10–12 alloying elements; therefore, they can be employed in applications where temperatures exceed 500 °C. These alloys typically operate within a range of 0.6–0.75 of their absolute melting point, which is in the proximity of the melting temperature of nickel (1455 °C) and cobalt (1495 °C). One of the aims of TBCs is to extend the temperature range at which components made from these superalloys can operate [59–63].

Ni-based superalloys can be classified into six generations of evolution based on the type and percentage of alloying elements, with the sixth being the most recently developed. The first generation of superalloys use a range of elements, including Ni, Co, Cr, Mo, Ti, W, etc. The second generation introduced the use of Re in proportions of 2 to 3% in order to improve creep strength. The first two generations were used to manufacture polycrystalline components, especially in the aerospace industry. The third generation highlights the increased use of Re up to 6%, marking the onset of the manufacturing of single-crystal components. The fourth generation of Ni-based superalloys was achieved through the introduction of Ru in order to facilitate the inclusion of other refractory elements. In the fifth generation, the concentration of Ru increases up to 6%, expanding the range of operating temperatures up to 1100 °C. The sixth generation enhances oxidation resistance by combining elements from previous generations with chemical elements such as Cr.

The last two generations are exclusively used in the production of single-crystal components. An important aspect to highlight is the limited research conducted on the application of TBCs on fifth and sixth-generation superalloys and the opportunity to study their potential impact on oxidation, creep or thermal behavior [64–66].

4.2. Bond Coat

In most cases, the TC layer is not directly deposited onto the substrate. Instead, an intermediate layer, the bond coat, is used, fulfilling several essential functions. It not only enhances the adhesion of the top layer to the component requiring thermal protection but also facilitates the behavior of both the TC layer and the substrate under thermal load, reducing the stress resulting from the different coefficients of thermal expansion (CTE) between the superalloy and the top ceramic layer. Additionally, this intermediate layer protects the substrate from corrosion and oxidation by forming a protective layer, typically α -Al₂O₃, known as TGO, due to the high concentration of reactive elements (e.g., Al) present in the BC [67,68].

Development, adhesion and TGO resistance are directly influenced by the composition of the BC. The specialized literature [69–71] identifies two main types of bond coating: (i) *MCrAlX* ($M = Ni$ and/or Co ; $X = Zr, Y, Hf$ and/or Si) coatings typically deposited using air plasma spray (APS), low-pressure plasma spray (LPPS), electron Beam–physical vapor deposition (EB-PVD) or high-velocity oxy-fuel (HVOF) and (ii) *diffusion-based aluminide coatings* deposited using electroplating/spark plasma sintering (SPS), chemical vapor deposition (CVD), etc.

(i) The first category is based on conventional MCrAlY-type coatings (at 900–1000 °C with β -NiAl and γ -Ni solid solution or γ' -Ni₃Al phases), which generally contain 10–30% Co, 15–25% Cr and 8–12% Al and have low thermal conductivity (12–15 Wm⁻¹K⁻¹). The four resulting combinations ensure good performance under high-temperature exposure

conditions due to their ability to form Al and Cr oxides. Thus, NiCrAlY offers superior oxidation resistance compared to CoCrAlY, which exhibits better resistance to hot corrosion, while NiCoCrAlY with CoNiCrAlY provides resistance properties to both thermal demands [72–75].

To enhance the formation mechanism and increase the adherence capacity of the formed TGO, reactive elements such as Y, Hf, Zr, La and Ce are associated with MCrAlY, usually in small amounts, below 1%. Additionally, the doping of refractory elements, such as Ta, Re, Ta/Re (usually <3%) or Si (usually <1%), enhances oxidation resistance [75]. Ogawa et al. [76] state that the addition of Ce improves the mechanical properties of CoNiCrAlY by enhancing the crack resistance of TBCs. Duan et al. [77] highlight that the addition of Hf reduces the CTE of the BC and slows down the growth rate of the TGO layer and, additionally, the incorporation of HfO₂ within the TGO layer inhibits the formation of defects. Another study [78] demonstrates that Hf/Ta co-doped into NiCoCrAlY BC significantly extends the lifespan of TBCs.

(ii) The second category is represented by the aluminides of Ni and Pt (Ni,Pt)Al initially used against hot gas corrosion without a ceramic topcoat. NiAl presents good oxidation resistance at 1200 °C and has a low density (5.9 g/cm³) and high melting temperature at 1638 °C [79]. A Pt layer with a thickness of 5–10 µm is applied via electrodeposition, followed by diffusion and aluminization. This type of bond coat ensures the formation of transient alumina and ultimately α-Al₂O₃ because of the high content of Al, up to 30%. The literature highlights that the inclusion of Ir and Ru enhances both hot corrosion resistance and creep strength due to their capacity to establish a barrier, thus inhibiting the diffusion of detrimental compounds toward the BC/TGO interface [72,80–83].

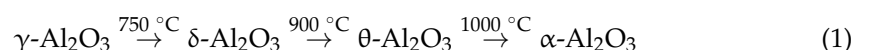
The thickness of the BC layer can vary depending on the composition used and the application but generally falls around approximately 100 µm [81]. Another important aspect is the roughness of the BC, which significantly influences the lifespan of the TBCs. Proper roughness aids in the adhesion of the TC with a uniform distribution of mechanical stresses, while excessive roughness can lead to stress concentrators that may cause cracking and delamination [84,85].

4.3. Thermally Grown Oxide

TGO forms in a thin layer at the interface between the BC and the TC layer in service conditions, due to BC oxidation under the influence of high temperatures exceeding 700 °C [86]. The further development of TGO is expected, and this process should occur in a controlled manner so that the TGO meets certain requirements [87,88], like:

- Good adhesion to both the metallic substrate and the upper ceramic layer to prevent delamination and spallation;
- Chemical stability at high temperatures to withstand harsh operating conditions;
- Mechanical resistance to static and dynamic loads, ensuring durability under stress;
- Slow, consistent and continuous growth (thickness ≤ 10 µm) to maintain structural integrity;
- The ability to generate suitable oxides to form an effective barrier against oxygen diffusion through the TC.

Depending on the composition of the BC, oxidation results in a range of oxides, among which the most common are chromia ((Cr,Al)₂O₃), spinel (Ni(Cr,Al)₂O₄), nickel oxide (NiO) and silica (Si₂O). Among these, the most important is alumina (Al₂O₃), especially in its α-Al₂O₃ phase, which develops as a result of a series of transformations, as shown in Equation (1) [88]:



Its development is crucial in TBC applications due to its excellent resistance to high temperatures and its chemical stability. Because of its relatively low diffusivity, it acts as a barrier against the penetration of oxygen from the harmful environment to the substrate [89].

In some cases, to prevent TBC failure, pre-oxidation treatment of the BC is performed before TC deposition with the aim of promoting the development of $\alpha\text{-Al}_2\text{O}_3$ with the desired characteristics [90].

4.4. Topcoat

The outer layer of TBCs, known as the TC, is designed to provide protection against the effects of high temperatures found in harsh working environments, safeguarding the metallic substrate and BC from deterioration, thus acting as an insulating layer. This layer is typically composed of ceramic materials that can be deposited through the use of various methods. The thickness of the topcoat can vary significantly depending on the application, ranging up to millimeters but typically falling between 100 and 600 μm [88,91–93].

The materials used in manufacturing the topcoat must meet several cumulative conditions to ensure optimal performance [80,88]:

- Low thermal conductivity for thermal insulation and a CTE similar to the substrate to reduce thermal stresses and the risk of delamination or cracking;
- Phase stability at high temperatures during prolonged exposure and thermal shock;
- Resistance to chemical attack by various compounds and chemical elements;
- Mechanical and thermodynamic compatibility with the TGO.

5. Topcoat Materials

Taking into consideration the variety of materials available and the possibility to combine them in various concentrations, this opens the way to a vast array of options, amounting to thousands of potential topcoats that can be utilized. Therefore, classification can be based on the general chemical form or the main constituents of materials. This method provides an organized and clear lane to navigate the vast array of materials, simplifying the understanding of their differences and applications.

A summary of the main materials described further by their chemical form can be found in Figure 4.

Chemical form	Simple oxides and defect-clustered materials
	Perovskites
	Pyrochlores
	Magnetoplumbite-type oxides

Figure 4. Classification of TC materials by chemical form.

A more complex classification, based on the main constituent, is illustrated in Figure 5, with each of these groups being detailed subsequently.

A. Simple Oxides and Defect-Clustered Materials

Simple oxides can be represented by the general chemical formula A_xO_y , where A stands for a metal cation and x and y are determined by the valency. Clusters, also known as nano-phases, refer to groups of atoms or molecules that have bound together to form a small distinct region. These clusters represent localized areas within a crystal lattice that contain a high concentration of point defects, such as vacancies and interstitial or substitutional atoms. Clusters are intentionally induced within the crystal structure through the addition of dopant oxides, which cause lattice distortions and promote local ionic segregation, leading to the formation of defect clusters. The most significant advantage of this is the reduction in thermal transfer of the topcoat, enhancing the material's efficiency as a thermal barrier [94].

Main constituents	Metallic and Rare Earth Oxides		
	Zirconates	Zirconia-Based Materials	Yttria-Stabilized Zirconia (YSZ/Y ₂ O ₃ -ZrO ₂)
			Calcia-Stabilized Zirconia (Ca-SZ/CaZrO ₃)
			Magnesia-Stabilized Zirconia (Mg-SZ/MgZrO ₃)
			Ceria-Stabilized Zirconia (Ce-SZ/CeO ₂ -ZrO ₂)
	Rare Earth zirconates (RE-Zirconates)		
	Rare Earth Niobates (RE-Niobates)		
	Rare Earth Tantalates (RE-Tantalates)		
	Other Materials	Mullite (porcellanite)	
		Aluminates	
		Silicates	
		Phosphates	
		High-Entropy Materials	

Figure 5. Classification of the most common TBC materials by their main constituents.

B. Perovskites

Perovskite materials follow the general formula ABO_3 for the simple form, where A and B are two different ions. The complex form, $A(B'_x B''_y)O_3$, represents a more complex perovskite structure, where B is shared by two different ions (B' and B'') in a specific ratio (x, y) [95]. Their main characteristic is their very high melting point (e.g., SrZrO₃—2650 °C; Ba(Mg_{1/3}Ta_{2/3})O₃—3100 °C) [96]. Moreover, incorporating ions with large atomic masses (lanthanides (such as La, Ce, Gd, Zr, Hf, etc.) can effectively reduce thermal conductivity. This is because the heavier ions vibrate at lower frequencies, resulting in slower phonon velocity, which is crucial for minimizing heat transfer [97].

C. Pyrochlores

Pyrochlore is characterized by its general formula $A_2B_2O_7$, where the A site is typically occupied by cations with a valence of +3 (such as rare earth lanthanides) and, in some cases, +2, while the B site hosts cations with a valence of +4 or +5 (Zr, Hf, Nb, Ta, etc.) [96]. Certainly, the A and B positions within the pyrochlore framework can host an array of elements in combination, allowing for a rich diversity beyond solitary elements.

These materials are known for their phase stability up to 1400 °C and their resistance to calcium–magnesium–alumino-silicate (CMAS) attack. However, challenges can arise due to mismatches in the CTE between the pyrochlore and the substrate material, potentially leading to stress within the coating [98].

D. Magnetoplumbite-Type Oxides

Magnetoplumbite-type oxides with the formula $LnMA_{11}O_{19}$ are promising for use in TBCs. In this formula, Ln covers lanthanides from La to Gd. The choice of Mg, Mn, Cr, Sm and Zn for M and either Al or Fe for A offers flexibility, making these materials adaptable for high-temperature applications. With their distinctive hexagonal structure, these materials combine structural integrity and thermal stability, enduring temperatures of up to 1600 °C [98,99].

Another more extensive description of these materials could be achieved by categorizing them into material groups.

5.1. Metallic and Rare Earth Oxides

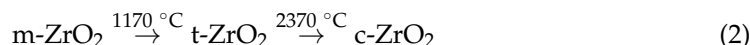
Some of the simplest forms of coatings, in terms of composition, consist of the common oxides of metals, such as alumina (Al_2O_3), zirconia (ZrO_2), chromia (Cr_2O_3), titanium dioxide (TiO_2), hafnium dioxide (HfO_2), etc., or rare earth oxides: yttrium oxide (Y_2O_3), lanthanum oxide (La_2O_3), cerium oxide (CeO_2), neodymium oxide (Nd_2O_3), etc. [100]. In some cases, some of these oxides can be used as standalone topcoats [101,102], but they are usually combined with each other or other elements [103–105] to enhance the phase stability and thermal and mechanical properties of the coating, giving rise to other groups of materials.

5.2. Zirconates

5.2.1. Zirconia-Based Materials

Zirconia (ZrO_2), one of the simplest zirconates and a commonly encountered oxide in TBCs, exhibits suitable properties for usage in coatings, such as a high melting point at $2700\text{ }^\circ\text{C}$, a CTE of approximately $10\text{--}11 \times 10^{-6}\text{ K}^{-1}$ and a thermal conductivity of $2\text{--}2.5\text{ Wm}^{-1}\text{K}^{-1}$ [106].

However, at high temperatures, zirconia undergoes phase transformations with volume changes of up to 8%, leading to undesired cracking in the coating. According to Equation (2), at a temperature of $1170\text{ }^\circ\text{C}$, the monoclinic phase (m- ZrO_2) transitions to the tetragonal phase (t- ZrO_2), followed by the appearance of the cubic phase (c- ZrO_2) at $2370\text{ }^\circ\text{C}$ [107,108].



To overcome these less favorable aspects, ongoing studies focus on enhancing performance through the use of various methods, including doping, multilayering, nanostructuring or functionally graded approaches [109].

To stabilize the t and m phases of zirconia at ambient temperature, a variety of oxides of metals and rare earth elements are used, typically CaO, MgO and CeO_2 , Y_2O_3 . To adjust the properties of materials according to specific application requirements, total stabilization with larger quantities of stabilizer or partial stabilization with smaller quantities is practiced. Total stabilization is preferred to achieve superior thermal and chemical stability, while partial stabilization is used when certain flexibility, higher resistance to mechanical stresses, thermal shocks, or specific chemical reactivity is needed [110].

5.2.1.1. Ytria-Stabilized Zirconia (YSZ/ $\text{Y}_2\text{O}_3\text{-ZrO}_2$)

The most common stabilizer of ZrO_2 is yttria (Y_2O_3), thus making YSZ the most popular coating material, which, over time, has become a reference in the specialized literature. Although YSZ can be found in various proportions of yttria stabilizer, the composition of 6 to 8% $\text{Y}_2\text{O}_3\text{-ZrO}_2$ or 7YSZ has been the most commonly studied variant since the late 1970s to the present day, with it being considered the optimal composition for most applications [111].

Regarding thermal properties, for 3–12% Y_2O_3 , the thermal conductivity was found to be $2.20\text{--}2.50\text{ Wm}^{-1}\text{K}^{-1}$ and the CTE was found to be $10.3\text{--}11 \times 10^{-6}\text{ K}^{-1}$, measured over the temperature range of $20\text{--}1000\text{ }^\circ\text{C}$ [112].

The addition of Y_2O_3 as a dopant has been observed to have a dual effect; it reduces the fracture toughness of the TC material while simultaneously promoting the formation of a tetragonal or cubic phase in the ZrO_2 matrix [107].

However, the phase remains stable up to temperatures of $1200\text{ }^\circ\text{C}$. Exceeding this threshold leads to volume changes, significant increases in thermal conductivity and, consequently, the accelerated diffusion of oxygen, resulting in TC delamination. Thus, classic YSZ coatings are limited to this threshold, which is unsatisfactory for advanced applications, especially within the aircraft sector [98].

A particular aspect related to degradation is highlighted by Vaßen et al. [113], who argue that prolonged exposure to high temperatures is not the cause of failure in YSZ coatings but rather the rate of cooling. Through an experimental study, they showed that a slow decrease in coating temperature, with a cooling rate below 10 °C/s, allows for the operation of YSZ coatings at a surface temperature of 1500–1550 °C.

Another method to enhance the utilization of YSZ is doping with various elements [114,115]. Yang et al. [116] report that doping zirconia with a compound consisting of Y₂O₃, TiO₂, Dy₂O₃, Gd₂O₃ and Yb₂O₃ can result in a coating that performs well at 1600 °C. At this temperature, the thermal conductivity of the coating was 1.5 Wm⁻¹K⁻¹.

Additionally, doping with Bi₂O₃ and CuO can have favorable effects on sintering, but with limitations induced by the destabilization of the crystalline structure of YSZ [117,118].

5.2.1.2. Calcia-Stabilized Zirconia (Ca-SZ/CaZrO₃)

Due to its perovskite structure, CaZrO₃ exhibits remarkable properties for its use in TBCs. This compound demonstrates excellent chemical stability at temperatures up to 1500 °C, with a melting point of 2550 °C [119,120]. Additionally, its thermal conductivity is low, with a value of approximately 2 Wm⁻¹K⁻¹. Its CTE at a temperature of 1000 °C is approximately 12.4 × 10⁻⁶ K⁻¹, indicating good thermal compatibility with the substrate and integration with other compounds for the TC [121].

Regarding the deposition method, Garcia et al. [120] demonstrate the sufficient processing of Ca-SZ through spraying techniques (air plasma spray and flame spray), achieving structures with extremely low thermal conductivity, below 0.5 Wm⁻¹K⁻¹ at 1000 °C, due to the porous structures obtained. In their study, Kumar et al. [122] identified good mechanical stress resistance in automotive engine cylinders using finite element analysis.

It may also be important to mention that the production of Ca-SZ offers cost efficiencies and increased availability when compared to YSZ [123].

The addition of CaZrO₃ to other elements used in coatings can have beneficial effects. Ejaz et al. [121] demonstrate that the use of Ca-SZ in combination with conventional YSZ (ZrO₂·8Y₂O₃) in a corrosive environment composed of 50% Na₂SO₄ and 50% V₂O₅ at temperatures of 950 °C prevents the destabilization of YSZ by forming CaV₂O₄ instead of YVO₄. This contributes to the extension of the TBC's lifespan.

5.2.1.3. Magnesia-Stabilized Zirconia (Mg-SZ/MgZrO₃)

Another perovskite structure that has been obtained is MgZrO₃. It exhibits good wear and corrosion resistance at high temperatures in moist environments with excellent performance at temperatures of 900 °C. It maintains chemical stability up to 1200 °C and has a melting temperature of 2140 °C. Also, it exhibits a thermal conductivity of 3 Wm⁻¹K⁻¹ and a CTE of 10 × 10⁻⁶ K⁻¹ measured over the range of 25–600 °C, making it suitable for coatings in applications with lower temperature intensities, such as exhaust nozzles, internal combustion engine components or molds due to its resistance to molten metals, particularly light ones such as aluminum, copper or zinc [124,125].

This material shows promising potential for application in SI engines, as Fouad et al. [126] conducted a finite element analysis covering the piston of a SI engine with various TC thicknesses using specific parameters for YSZ, MgZrO₃, alumina and mullite. The increase in TC thickness directly influences the temperature rise on the piston surface and is inversely proportional to the substrate temperature. MgZrO₃ has been reported to perform the best, for the maximum TC thickness of 1.6 mm, reducing the substrate temperature by almost 7% and increasing the surface coating temperature by over 140%, which favors combustion.

Also, it may be evident that the use of MgO in combination with other elements can lead to the optimization of coating systems. Azhar. et al. [127] reported that adding MgO to zirconia-toughened Al₂O₃ (ZTA) enhances its hardness and boosts wear resistance by 50%. Yamagata et al. [128] experimentally demonstrated that doping ZrO₂ with Y₂O₃-MgO completely stabilizes the cubic phase and additionally increases hardness.

5.2.1.4. Ceria-Stabilized Zirconia (Ce-SZ/CeO₂-ZrO₂)

CeO₂ is added to ZrO₂ primarily to decrease thermal conductivity and increase CTE, to bring it closer to the behavior of the substrate. Gul et al. [129] show that doping at a concentration of 8% Ce is sufficient for a significant reduction in thermal conductivity.

Following a comprehensive study on the properties of a plasma-sprayed Ce-SZ coating, Sodeoka et al. [130] demonstrate that for a concentration of 50 mol% CeO₂, the thermal conductivity is below 0.5 Wm⁻¹K⁻¹ and the CTE is around 12.5 × 10⁻⁶ K⁻¹, measured over a range of ambient temperature up to 800 °C. Additionally, above 1000 °C, the compound appears to lose its insulating properties due to sintering. In their study, Mousavi et al. [131] demonstrate that air plasma-sprayed CSZ exhibits good corrosion resistance in Na₂SO₄ + V₂O₅ salt environments at temperatures of 950 °C when deposited on a BC obtained through spark plasma sintering. Adding to this, Keyvani et al. [132] highlight that the nanostructured combination Al₂O₃/Ce-SZ presents better resistance than conventional YSZ and CSZ in saline environments at temperatures of 1050 °C. In another study, Krogstad et al. [133] reported that co-doping ZrO₂ with CeO₂ and TiO₂ offers a way to simultaneously improve toughness and phase stability at temperatures of 1350 °C.

5.2.2. Rare Earth Zirconates (RE-Zirconates)

In addition to the perovskite structure, rare earth zirconates can also form combinations in the form of pyrochlores. The general form for these materials is RE₂Zr₂O₇, where RE = lanthanide group, especially La, Nd, Sm and Gd, which form the most used compositions for TBCs [134]. It is important to note that rare earth zirconates come in a variety of types, with some having complex chemical compositions or being improved by adding other elements. Therefore, the chemical formula can change based on the precise composition.

Due to their composition and structure, RE zirconates exhibit high melting points, low thermal conductivity and chemical stability at high temperatures, which can exceed 1400 °C [135].

One issue could be the relatively low CTE, which may induce stress in the coating, leading to a decrease in the number of operating cycles. One potential solution could be the utilization of a multilayer coating strategy [136].

The thermal characteristics of some RE-zirconates are provided in Table 1 [137,138].

Table 1. CTE and thermal conductivity of RE-Zirconates (data from Refs. [137,138]).

Material	CTE (10 ⁻⁶ K ⁻¹)	Thermal Conductivity at 1200 °C (Wm ⁻¹ K ⁻¹)
Lanthanum zirconate (La ₂ Zr ₂ O ₇ , LZ)	9.1	1.98
Samarium Zirconate (Sm ₂ Zr ₂ O ₇ , SZO)	10.8	2.09
Neodymium Zirconate (Nd ₂ Zr ₂ O ₇ , NZO)	9.5	1.83
Gadolinium Zirconate (Gd ₂ Zr ₂ O ₇ , GZO)	11.6	1.91

These properties can be improved by creating more complexly doped zirconate structures. Zhou et al. [139] formed structures of La₂Zr₂O₇ doped with Dy₂O₃, Nd₂O₃ and CeO₂. Following testing, the materials obtained exhibited lower thermal conductivity and improved CTE compared to undoped zirconate and in some cases even better CTE than the classic 8YSZ.

High-entropy materials could also represent a promising option. In their study, Li et al. [140] prepared high-entropy coatings with a pyrochlore structure represented as (5RE_{0.2})₂Zr₂O₇ where 5RE can consist of combinations of five rare earth oxides out of the following: La₂O₃, Nd₂O₃, Sm₂O₃, Eu₂O₃, Gd₂O₃ and Y₂O₃. All combinations exhibited thermal conductivity about 50% lower than that of traditional YSZ, below 1 Wm⁻¹K⁻¹, over the range of 300–1200 °C. Liu et al. [141] also reported improved mechanical properties for the high-entropy coating (La_{0.2}Nd_{0.2}Sm_{0.2}Gd_{0.2}Yb_{0.2})₂Zr₂O₇, with a thermal conductivity of 0.9–1.72 Wm⁻¹K⁻¹ over the range of 0–1000 °C and an increased CTE of 10.9 × 10⁻⁶ K⁻¹ at 1000 °C.

Aspects related to high-entropy coatings will be briefly summarized below in this section.

5.3. Rare Earth Niobates (RE-Niobates) and Tantalates (RE-Tantalates)

Niobate and tantalate can be found in coatings in various forms, but due to their properties, they are mostly encountered alongside rare earth elements, forming two classes of materials: rare earth niobates and rare earth tantalates. Of course, they can be found in various chemical forms, but due to their high melting points, the forms RE_3NbO_7 , RENbO_4 , RETaO_4 , RE_3TaO_7 and RETa_3O_9 are the ones used in TBCs [142,143].

An interesting aspect is highlighted by Yang et al. [144], who demonstrate that simple combinations under the structure RE_3NbO_7 , formed from rare earth oxides RE_2O_3 ($\text{RE} = \text{Dy}, \text{Er}, \text{Y}, \text{Yb}$) and niobium oxide (Nb_2O_5), but with significant internal chemical inhomogeneities caused by charge disorder and bond fluctuation, can exhibit better properties than YSZ and even better properties than complex structures containing multiple elements, such as high-entropy ones. The thermal conductivity at 1000 °C is half that compared to YSZ, with values ranging between 1.25 and 1.5 $\text{Wm}^{-1}\text{K}^{-1}$.

In a follow-up study, Yang et al. [145] determined good CTE values for these combinations ranging between 9 and 11 $\times 10^{-6} \text{K}^{-1}$ at 1000 °C. Additionally, Dy_3NbO_7 and Y_3NbO_7 exhibit enhanced resistance to CMAS attack compared to 7YSZ. An issue requiring further investigation are fracture toughness and hardness, which recorded lower values than those of YSZ.

For the RENbO_4 compound ($\text{RE} = \text{Y}, \text{La}, \text{Nd}, \text{Sm}, \text{Gd}, \text{Dy}$ and Yb) tested by Wu et al. [146], thermal conductivity values of 1.42–2.21 $\text{Wm}^{-1}\text{K}^{-1}$ were achieved, measured over the range of 500–900 °C, along with a CTE of 9.8–11.6 $\times 10^{-6} \text{K}^{-1}$. Improvements in properties are suggested by Zhang et al. [147], who report that, through lattice distortion, the CTE of RENbO_4 can reach values of 12.8 $\times 10^{-6} \text{K}^{-1}$.

Regarding compounds containing tantalum, the thermal characteristics are highlighted in Table 2 [143].

Table 2. CTE and thermal conductivity of RE-Tantalates (data from Ref. [143]).

Compound	CTE (10^{-6}K^{-1})	Thermal Conductivity ($\text{Wm}^{-1}\text{K}^{-1}$)
RETaO_4	5.2–10.7	1.27–7.92
RE_3TaO_7	6.1–10.5	1.20–1.97
RETa_3O_9	4.1–9.6	1.17–2.41

It can be observed that a problem with tantalates is their low CTE, particularly in the case of RETa_3O_9 , leading to bonding mismatches.

Based on a study conducted on RETa_3O_9 ($\text{RE} = \text{Ce}, \text{Nd}, \text{Sm}, \text{Eu}, \text{Gd}, \text{Dy}$ and Er), Chen et al. [148] assert that this parameter is highly dependent on the rare earth element used, with the study showing higher values for CeTa_3O_9 .

However, the negative aspects of RE_3TaO_7 and RETa_3O_9 are given by their low fracture toughness, with values of 1.0–2.6 $\text{MPa}\cdot\text{m}^{1/2}$, below the YSZ reference (3.5 $\text{MPa}\cdot\text{m}^{1/2}$), which makes the topcoats prone to failure. On the other hand, RETaO_4 and RENbO_4 show high fracture toughness of 2.4–3.8 $\text{MPa}\cdot\text{m}^{1/2}$, which makes them some of the best coating structures [143]. Additionally, Chen et al. [149] highlight the potential use of RETaO_4 ($\text{RE} = \text{Yb}, \text{Lu}$ and Sc) in the monoclinic-prime (m') phase at high temperatures, with the compounds showcasing remarkable compatibility with alumina and maintaining their structure without phase transition up to temperatures of 1500 °C. It should be also noted that the CTE exhibited ($3\text{--}8 \times 10^{-6} \text{K}^{-1}$ in the range 200–1200 °C) is not entirely satisfactory.

5.4. Other Materials

5.4.1. Mullite (Porcellanite)

Mullite is a relatively simple material consisting of silica (SiO_2) and alumina (Al_2O_3) in the form of ($3\text{Al}_2\text{O}_3\cdot 2\text{SiO}_2$). It is used as a coating material due to its low density and

resistance to corrosion and creep [150]. Its thermal properties include a melting point of 1880 °C, thermal conductivity of $3.5 \text{ Wm}^{-1}\text{K}^{-1}$ and a relatively low CTE of $5.3 \times 10^{-6} \text{ K}^{-1}$ at 1000 °C [151]. At temperatures of 1000 °C, the amorphous phase of mullite transitions into crystalline form accompanied by volume contraction, which can lead to the failure of the TBC [152]. Although it is not favorable for use in applications with extremely high temperatures, it exhibits excellent insulation and corrosion protection performance at lower temperatures, such as in industrial incinerators or internal combustion engines in automotive or naval applications [153,154].

5.4.2. Aluminates

Rare earth aluminates, mostly found in the form of $\text{RE}_4\text{Al}_2\text{O}_9$ and rare earth hexaaluminates with the general formula $\text{AB}_x\text{Al}_{12-x}\text{O}_{19}$ (A = Na, Ba, La, Ca, Sr and Ce; B = transition metal or noble metal ion) are the most representative in this group, with use in applications that can exceed 1300 °C on the surface of components [155,156]. $\text{LaTi}_2\text{Al}_9\text{O}_{19}$ exhibits phase stability up to 1600 °C, a thermal conductivity of $1.0\text{--}1.3 \text{ Wm}^{-1}\text{K}^{-1}$, measured from 300 to 1500 °C, and a promising CTE of $11.2 \times 10^{-6} \text{ K}^{-1}$, measured from 200 to 1400 °C [157]. Another commonly encountered aluminide is $\text{Y}_4\text{Al}_2\text{O}_9$, which exhibits chemical stability up to 1300 °C and a thermal conductivity of $1.81 \text{ Wm}^{-1}\text{K}^{-1}$ at 1000 °C but with a relatively low CTE ($8.91 \times 10^{-6} \text{ K}^{-1}$) [158].

5.4.3. Silicates and Phosphates

Silicates and phosphates are less commonly used in TBCs due to their low CTE. However, they may be found in environmental barrier coatings (EBC) as protection against CMAS attack [159,160].

5.4.4. High-Entropy Coatings (HECs)

High-entropy coatings, derived from high-entropy alloys, are a recent subject in specialized literature. These coatings are based on the principle that a higher level of atomic disorder can lead to a more distorted crystal lattice. This complexity can inhibit the movement of dislocations, thereby enhancing the mechanical properties and decreasing thermal conductivity compared to traditional materials. High-entropy coatings (HECs) are a blend of five or more elements, usually added in similar quantities, to combine the properties of all constituents. Despite the presence of multiple elements, high-entropy oxides maintain a single-phase crystal structure, contributing to their unique properties. Even though HECs are a recent topic, numerous functional variants have already been discovered [161,162].

In their study, Yao et al. [163] present findings on a series of zirconia-based ceramics with the formula $\text{Zr}_{1-4x}\text{Y}_x\text{Yb}_x\text{Ta}_x\text{Nb}_x\text{O}_2$, where $x = 0.2, 0.172, 0.142, 0.114$ and 0.083 . They achieved remarkable thermal properties, including a thermal conductivity of around $1.37 \text{ Wm}^{-1}\text{K}^{-1}$ at 900 °C and a CTE of $11.3 \times 10^{-6} \text{ K}^{-1}$ at 1000 °C. Moreover, the material demonstrated good toughness, reaching up to about $4.59 \text{ MPa}\cdot\text{m}^{1/2}$. The compound also exhibited stability up to 1600 °C and good resilience against degradation by CMAS.

According to the study conducted by Hsu et al. [164], high-entropy materials may have multifunctional potential in TBC systems. They explored the capabilities of the alloy $\text{NiCo}_{0.6}\text{Fe}_{0.2}\text{Cr}_{1.5}\text{SiAlTi}_{0.2}$, highlighting its suitability, particularly as a bond coat. This compound can form a protective $\alpha\text{-Al}_2\text{O}_3$ layer at 1100 °C, offering enhanced thermal stability and reduced thermal conductivity, along with a lower CTE compared to the traditional MCrAlY bond coat.

6. Design of TBCs

The properties of TBCs are tied to their design, emphasizing the importance of judiciously selecting coating techniques, optimizing structural density and strategically structuring layers to fulfill diverse functional requirements.

These aspects determine the adhesion between layers, thermal protection and overall lifespan. These considerations play a pivotal role in tailoring TBCs to meet specific performance criteria and effectively address the varied demands of their intended applications.

6.1. Coating Techniques

The diversity of available coating techniques is vast. The choice among these processes depends on the precise engineering needs, balancing factors such as coating thickness, bond strength, thermal properties generated, cost-effectiveness to achieve the optimal outcome, as well as their environmental impact.

A brief categorization of the coating techniques commonly used can be found in Figure 6 [165,166] at the end of this section.

6.1.1. Air Plasma Spray (APS)

APS stands out as a preferred coating technique due to its simple setup with atmospheric operation, cost efficiency and adaptability, suitable for both metallic and refractory ceramic materials. The process predominantly uses powdered materials as feedstock. Within this process, a carrier gas propels the material's particles at high speeds into the plasma, where they melt or semi-melt into droplets that adhere and crystallize on the target surface [167,168].

APS coatings are characterized by flattened, lamellar particles known as "splats" and micro-cracks parallel with the substrate. Such a formation is less resistant to thermal and mechanical stress. The key factors for this vulnerability are the inter-splat boundaries and cracks alignment, which facilitate the propagation of heat and stress, making the coating more susceptible to degradation. The porosity of the coating ranges from 5% to 25%, contributing to a thermal conductivity of $0.8\text{--}1.0\text{ Wm}^{-1}\text{K}^{-1}$. Typically, this coating has a thickness of $250\text{--}300\text{ }\mu\text{m}$, although in certain industrial gas turbine engines, it can extend up to $600\text{ }\mu\text{m}$, providing enhanced protection and performance [169–171].

To increase the durability of APS coatings, a relatively high but moderate surface roughness is necessary to enhance the adhesion surface area [169].

The APS technique is commonly selected for applying TBCs on stationary turbine components like combustors and vanes, areas with lower temperatures and for larger parts, owing to its cost-effectiveness and high deposition rates [10].

6.1.2. Electron Beam–Physical Vapor Deposition (EB-PVD)

In the EB-PVD process, a powerful electron beam is used to vaporize the coating material (target) within a protected atmosphere inside a vacuum chamber (pressure below 10^{-2} Pa). Magnetic fields and a high voltage direct the electron beam to the target surface. As this vapor traverses the chamber, it deposits and crystallizes on the substrate, yielding a uniformly thin coating [172]. The resulting structure is columnar/feather-like columnar, with a thermal conductivity of up to $1.7\text{ Wm}^{-1}\text{K}^{-1}$ [173].

EB-PVD coatings are regarded as more durable than those applied via APS, a distinction that is largely due to the unique microstructural features of EB-PVD coatings, specifically the formation of inter-columnar voids within the structure. These voids confer three major benefits: they impart flexibility to the coating during thermal cycling, which helps mitigate the mismatch in the CTE between the coating and the BC or substrate. This leads to increased fracture toughness in the coating. Additionally, they act as crack deflectors, preventing the spread of cracks parallel to the substrate that could lead to delamination [167,169]. The structure is quite porous due to the gaps between columns, the feather-like appearance and pores within the columns, which disrupt heat flow, making it more challenging for heat to pass through the coating [174].

A significant drawback limiting wider application is the high cost of the equipment required. EB-PVD is applied to technologically precise parts where the surface to be coated must be smooth, as it even adheres to fine surfaces, unlike APS, due to chemical bonding, resulting in much thinner layers than APS. It is typically used for parts subjected to high thermal and mechanical stress, which are in motion [10,167].

6.1.3. Suspension Plasma Spraying (SPS)

In SPS, the raw material consists of an extremely fine mixture of either ceramic or metal particles (nanometers to micrometers) suspended in a liquid medium, often water or alcohol. The suspension is injected into a plasma torch where the liquid carrier quickly evaporates, allowing the plasma jet to melt the tiny particles, which subsequently adhere to the substrate upon contact [175].

SPS merges the characteristics of both APS and EB-PVD, offering a relatively low-cost alternative to EB-PVD. It achieves a finer structure compared to APS, enhancing coating quality. SPS's adaptability, influenced by spray parameters and the formulation of the suspension, enables it to produce coatings with a wide range of porosities. This includes achieving highly porous coatings beyond what APS or EB-PVD typically offer, even over 50% [176]. Remarkably, SPS can create columnar structures, similar to EB-PVD or cauliflower-like structures, providing enhanced strain tolerance and better thermal fatigue strength than coatings applied via APS [177–179].

Bernard et al. [180] showed in their study on YSZ coatings the possibility of developing columnar structures via both SPS and EB-PVD techniques. Through the fine-tuning of processing parameters, they achieved a notable decrease in thermal conductivity: $1.3 \text{ Wm}^{-1}\text{K}^{-1}$ in YSZ coatings applied using EB-PVD and $0.7 \text{ Wm}^{-1}\text{K}^{-1}$ for those applied with SPS, measured at $1100 \text{ }^\circ\text{C}$.

Costly PS-PVD and SPS coating techniques can be effectively rivaled by APS by selecting appropriate materials and operational settings. Kubaszek et al. [173] demonstrated this with APS, applying $\text{ZrO}_2 \times 8\text{Y}_2\text{O}_3$ oxide powders. They used micrometric particles ($<10 \text{ }\mu\text{m}$) to produce $100 \text{ }\mu\text{m}$ thick coatings with about 8% porosity and nanometric particles ($<1 \text{ }\mu\text{m}$) to achieve $40 \text{ }\mu\text{m}$ thick coatings with 16% porosity. Using 7-8YSZ particles ranging from 50 to 150 nm , Gao et al. [181] achieved with APS a thermal conductivity of $0.8\text{--}0.95 \text{ Wm}^{-1}\text{K}^{-1}$ across temperatures of $300\text{--}450 \text{ }^\circ\text{C}$.

Physical Vapor Deposition (PVD)	Electron Beam–Physical Vapor Deposition (EB-PVD)		
	Pulsed Laser Deposition (PLD)		
Chemical Vapor Deposition (CVD)	Sol–Gel Processing		
	Metal–Organic Chemical Vapor Deposition (MOCVD)		
Thermal Spray Methods	Flame Spraying (FS)		
	Solution Precursor Plasma Spray (SPPS)		
	High-Velocity Oxy-Fuel (HVOF)		
	Detonation Gun Spraying (D-Gun)		
	Plasma Spraying (PS)	Suspension Plasma Spraying (SPS)	
		Air Plasma Spraying (APS)	
		Low-Pressure Plasma Spraying (LPPS)	
		Vacuum Plasma Spraying (VPS)	Plasma Spraying–Physical Vapor Deposition (PS-PVD)
		Plasma Spraying–Chemical Vapor Deposition (PS-CVD)	

Figure 6. Classification of the most common TBC processing methods (data from Refs. [165,166]).

6.2. Porosity

Porosity is an aspect that must be considered in the design of TBC as it influences the properties and performance of the coating. It does not represent a defect or a vulnerability in TBC as long as it is controlled. Porosity decreases the material's density, impacting its mechanical and thermal behaviors. Subjecting ceramic coatings to prolonged high temperatures can stimulate grain enlargement and aid in the repair of micro-cracks, which is beneficial in certain scenarios. This process also contributes to a reduction in porosity. A decrease in porosity leads to an increase in the elastic modulus, hardness and fracture toughness, but it increases the thermal conductivity. Hence, controlling porosity is essential for balancing thermal and mechanical properties, making the selection of the coating process crucial [182].

Generally, employing finer powder particles (under 50 μm) for coatings decreases porosity due to particle agglomeration [183]. The porosity of a standard TBC typically stands at around 15% [10]. For porosities exceeding 20%, poor erosion resistance has been reported, with high-porosity TBCs having more limited use [184]. On the other hand, thermal conductivity can be reduced to as low as $0.4 \text{ Wm}^{-1}\text{K}^{-1}$ when the porosity level is increased beyond 30% [176].

Thermal transport in TBCs is influenced by the thermal conductivity of the coating material and the gas trapped in the formed pores. In coatings produced via plasma spraying (PS), the gas conductivity within the pores can reach $0.025 \text{ Wm}^{-1}\text{K}^{-1}$. As the pores become finer, thermal conductivity decreases, reaching as low as $0.01 \text{ Wm}^{-1}\text{K}^{-1}$ for pore sizes of around 1 μm , even at coating temperatures exceeding $1700 \text{ }^\circ\text{C}$ [185].

6.3. Multi-Layer Topcoat

The concept of a topcoat composed of multiple layers of different materials, each stacked upon another and serving distinct functions, is a foundational principle in the development of advanced TBCs. This multi-layer strategy enhances the overall performance of the coating by leveraging the unique properties of each material layer. The benefits include enhanced mechanical, thermal and chemical resistance, the creation of diffusion barriers or the mitigation of CTE mismatch [186].

A good example is the case of zirconates with reduced CTE, with the combination with YSZ being commonly encountered. In their study, Liu et al. [187] compared electron beam–physical vapor deposited YSZ/LaYZrO double-ceramic and LaYZrO single-ceramic coatings on a NiCoCrAlYHf bond coating. Thermal performance was assessed through heating at $1150 \text{ }^\circ\text{C}$ and subsequent cooling cycles. The durability of the double-layer coating was found to be approximately 8 times greater than that of LaYZrO alone. LaYZrO exhibits low thermal conductivity (app. $1.6 \text{ Wm}^{-1}\text{K}^{-1}$ at $1000 \text{ }^\circ\text{C}$) and a low CTE (app. $9.3 \times 10^{-6} \text{ K}^{-1}$ at $1000 \text{ }^\circ\text{C}$), while YSZ was effective in mitigating the CTE mismatch with the bond coat. However, the increase in TGO and topcoat cracking requires careful consideration.

In their study, Mahade et al. [188] examined the oxidation behavior of double and triple multi-layer coating systems YSZ/ $\text{Gd}_2\text{Zr}_2\text{O}_7$ and YSZ/ $\text{Gd}_2\text{Zr}_2\text{O}_7/\text{Gd}_2\text{Zr}_2\text{O}_7$, created via suspension plasma spraying on NiCoCrAlY bond coats when exposed to $1150 \text{ }^\circ\text{C}$. The multi-layer systems exhibited lower TGO thickness compared to single-layer YSZ coatings, indicating better oxidation resistance. After exposure, the triple-layer system showed the lowest porosity, enhancing the barrier against oxygen penetration to the bond coat. Furthermore, both multi-layer coatings maintained good microstructural integrity, featuring vertical cracks and pores beneficial for absorbing thermal stresses. In a more recent study on double-layered YSZ/ $\text{Gd}_2\text{Zr}_2\text{O}_7$, Mahade et al. [189] demonstrated that over a certain thickness of YSZ, the durability of TBC decreases under thermal exposure, possibly due to stress caused by too large a difference in CTE. YSZ exhibits higher conductivity and absorbs more heat.

6.4. Functionally Graded Thermal Barrier Coatings

Advanced TBC systems known as functionally graded thermal barrier coatings (FGT-BCs) have a progressive change in composition and structure across the coating's thickness. In contrast to conventionally defined layer counts, FGTBCs do not have a set number of layers but are made with the intention of having a material property gradient from the substrate to the outside [190].

They are designed with flexibility, where chemical composition and crystalline structure, mechanical attributes like Young's modulus, shear modulus, material density and thermal properties such as thermal conductivity, the CTE, etc. transition smoothly across the coating in specified orientations. These coatings are ingeniously developed to mitigate the impacts of mechanical and thermal stresses, as well as thermal shock, chemical degradation and corrosion, enhancing the coating's overall resilience and longevity [191,192].

7. Degradation and Failure of TBCs

Regarding negative changes that may occur during the operation of components protected with TBC, they can manifest in the form of *degradation* and *failure*. Degradation refers to the physical or chemical changes that occur within the TBC structure as a result of exposure to extreme temperatures and stress, diminishing the insulation and protective capabilities over the substrate.

Failure refers to the loss of functionality or the inability of the TBC material to fulfill its purpose and it is considered when the BC is exposed to a harsh environment because a significant part of the TC has split off [91]. In both cases, monitoring and understanding the mechanisms that generate them and through which they manifest are essential for the efficient design and implementation of TBCs.

7.1. TGO Growth

As previously mentioned, oxidation at high temperature is the process responsible for forming the TGO diffusion barrier at the BC/TC interface, resulting from the reaction between oxygen and the reactive elements of the BC, with a specific focus on the formation of $\alpha\text{-Al}_2\text{O}_3$.

Following experimental observations, it was found that the growth of TGO is a diffusion-controlled process that follows a parabolic law given by Equation (3):

$$\delta^2 = k_p \times t \text{ [}\mu\text{m]} \quad (3)$$

where δ^2 is the TGO layer thickness, k_p represents the growth rate constant of TGO (measured in $[\mu\text{m}^2/\text{h}]$ and influenced by the oxidation system and BC constituents) and t is the oxidation exposure time [193,194]. The growth rate of the TGO is not constant over time; instead, it decreases with its thickening due to the accumulation of protective oxides that hinder oxygen diffusion toward the BC [91]. Controlling the growth of TGO is crucial because, once its thickness reaches 5–10 μm , it becomes a problematic phenomenon that significantly impacts the lifespan of the TBC [195]. Dong et al. [196] and Ding et al. [197] observed that an increase beyond the threshold of 5 μm of TGO thickness significantly reduces the lifetime of the TBC, decreasing exponentially even by up to 90%. On the other hand, Torkashvand et al. [198] demonstrate that a TGO thickness of 2–3 μm can be enough to provide protection against thermal shock. Therefore, uncontrolled oxidation of the BC, along with the excessive growth of TGO, can lead to excessive stress and reduced adhesion between layers which can result in *delamination* and *spallation*.

The stages of delamination and spallation phenomena are illustrated in Figure 7.

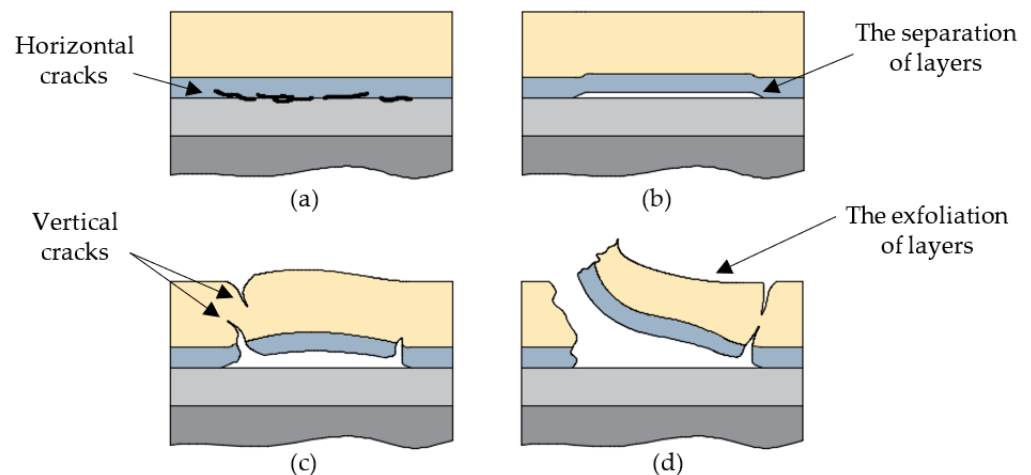


Figure 7. The stages of delamination and spallation phenomena: (a) the occurrence of horizontal cracks; (b) delamination; (c) the occurrence of vertical cracks; (d) spallation.

Delamination is the process by which individual layers of the TBC separate from each other due to cracks propagating parallel to the surface, occurring at the edges or corners of the component (edge delamination) or internally, causing wrinkles on the surface of the TBC (buckling delamination).

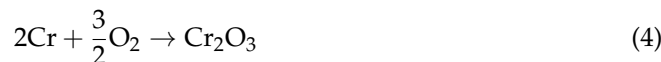
Spallation is the process by which layers peel off through brittle rupture mechanisms and depart from the surface on which they were deposited, with the cracks this time being transverse through the coating layers [199]. In general, delamination serves as a precursor to spallation. Specifically, buckling delamination weakens the TBC structure and reduces adhesion between layers, leading to the formation of transverse cracks and facilitating exfoliation [200]. Spallation can occur at both the TC/TGO interface and the TGO/BC interface. Typically, a thicker TGO layer may result in the displacement of the spallation plane toward the TGO/BC interface due to significantly higher residual stress in this region and reduced adhesion [194,201].

Stress can be generated by multiple sources, including external loads, vibrations, deformations, thermal cycling or shock to which components are subjected during operation. In this section, the focus is on that induced by the development of TGO. From this perspective, the existence of a cumulative stress can be considered, which includes: (a) growth stress found within the TGO due to the volumetric expansion of high-density metals and their transformation into low-density oxides; (b) CTE mismatch between TC/TGO and/or TGO/BC evident during heating–cooling cycles [194,202,203]. Evans et al. [204] highlight the fact that TGO exhibits residual compressive stress at ambient temperature, resulting from the differences in the CTE of the TC ($11\text{--}13 \times 10^{-6} \text{ K}^{-1}$ for $\text{ZrO}_2/\text{Y}_2\text{O}_3$), TGO ($8\text{--}9 \times 10^{-6} \text{ K}^{-1}$ for $\alpha\text{-Al}_2\text{O}_3$), BC and a Ni-based alloy substrate ($13\text{--}16 \times 10^{-6} \text{ K}^{-1}$).

7.2. Aluminum Depletion

Aluminum depletion is a type of chemical failure, referring to the process in which the Al content in the BC is reduced during high-temperature operation, determining spallation [205]. One of the causes can be the consumption of available Al in the BC through oxidation and the decrease in its concentration below the threshold necessary to sustain the formation of $\alpha\text{-Al}_2\text{O}_3$. At this point, there is favored accelerated association of other elements in the BC (Cr, Ni and Co) with O_2 , leading to the rapid growth of oxides, generically called spinels, which are much bulkier and more brittle, accentuating stress in the TGO. The formation occurs either through direct reaction or through the decomposition of already formed Al_2O_3 , leading to its complete or partial replacement with oxides such as NiO, CoO, Cr_2O_3 and $(\text{Ni, Co})(\text{Cr, Al})_2\text{O}_4$, which allow deep oxidation

of the BC, reducing the insulating capacity of the TBC system [203,206–208]. The reactions (4)–(8) below describe the formation mechanisms of certain oxides [208]:



On the other hand, in some situations, the controlled growth of these oxides can have beneficial effects, such as forming an additional protective barrier or reducing thermal conductivity. Taylor et al. [209] reported that the formation of Cr_2O_3 provides resistance to type I (900 °C) and type II (700 °C) hot corrosion in TBCs. Nevertheless, Berthod [210] and Eriksson [211] underline that exposure to temperatures above 1000 °C causes chromia to evaporate due to its volatility, decomposing into CrO_3 . Regarding the deep (internal) oxidation of the BC, Wang et al. [212] observed that the presence of oxides within the BC is characterized by the existence of isolated oxidized zones that can have positive effects by reducing the thickening and implicit the stress of TGO, as the formation of oxides is distributed within the BC. Additionally, the oxidized zones decrease the rate of crack propagation. Still, Zou et al. [213] mention that the benefits of internal oxidation are minor compared to the negative effect it has on the durability of the TBC.

Another cause that can lead to aluminum depletion is interdiffusion occurring at high temperatures when Al diffuses into the substrate, leading to the formation of voids that reduce the bonding between the BC and superalloy. This phenomenon can be mitigated by creating a diffusion barrier through the addition of refractory elements such as Ta and Re [214,215].

7.3. Sulfur Segregation

The presence of impurities, even chemical elements, leads to a decrease in the adhesion of TBC layers, resulting in spalling. The most problematic situation is the segregation of sulfur at the BC/TGO level in the voids resulting from alumina formation. Sulfur can be introduced into TBCs from various sources such as raw materials used in substrate and bond coat production, turbine or engine fuels or environmental pollution interacting with the components during operation [216,217].

The effect of sulfur segregation can be reduced by using desulfurized superalloys and by adding reactive elements such as Zr, Y or Pt along with Hf [218,219]. Smialek et al. report that superalloys perform well at an extremely low S concentration < 10 ppm; however, desulfurization to a concentration below 1 ppm of S significantly favors adhesion [220].

7.4. Foreign Object Damage and Erosion

Foreign object damage (FOD) represents a critical issue, especially for aircraft, as hard foreign objects, generally larger than 100 μm , (sand, rocks, birds, etc.) can penetrate open turbines, potentially damaging the TBC or the entire component [221,222]. FOD can cause various forms of damage, including erosion, delamination, spallation, mechanical deformation or even penetration (pitting) of the TBC, resulting in material loss, material fracturing and local thermal stress. Additionally, the affected areas retain residual stresses due to the shock, serving as crack propagation origins [223]. In their transit, the particles are heated by the combustion environment and entrained by the motion of the blades can break into small fragments that become projectiles damaging, in particular, jet engine blades and nozzle guide vanes.

Erosion is the physical process of deterioration caused by abrasion resulting from the impact of solid or semi-melted particles striking the surface of the TBC, compromising its functionality and durability. The level of degradation induced depends on particle properties (size, velocity, temperature, solid or molten state, etc.), the angle of impact and the microstructure of the TBC [224]. Particles smaller than 2 μm have a minor erosive effect, while those between 10 and 20 μm impact the back of the airfoil, whereas those $>40 \mu\text{m}$ affect the leading edges of the blades [225]. The speed at which the particles are carried varies depending on the speed of the blades and the size of the particles; therefore, as their size decreases, the speed increases, reaching up to 350 m/s [225,226]. Chen. et al. [227] specify that particles heated to 1450 °C impact the surface at a velocity of 10 m/s, including those measuring 560 μm , and at 170 m/s, those of 50 μm in size.

Protection against FOD is typically achieved at the turbine's construction level by incorporating filters or protective elements.

7.5. Corrosion and CMAS Attack

Corrosion is the chemical process of deterioration that commonly occurs during turbine operation, where the TBC is affected by reactions with substances present in the working environment, such as oxides, salts, gases or vapors containing corrosive compounds, which are deposited on the surface of components. Corrosive compounds can originate from different sources, such as low-quality fuel, atmospheric pollution, FOD, etc. [222]. High temperature plays a significant role in the occurrence of corrosion because, in most cases, TBC layers are penetrated by corrosive particles in a molten state. Solid particles are less commonly encountered in this phenomenon [228]. At temperatures exceeding 680 °C, hot corrosion will cause the oxidation of the TBC. Oxygen will penetrate through the pores of the TC and may diffuse deeply into the BC, potentially leading to the destruction of the protective oxide layer [229]. Hot corrosion occurs in stages, beginning with initiation, when salts reach the surface of the component and break the protective oxide layer, creating conditions for the propagation of the attack, thus distinguishing between type I hot corrosion at high temperature, above the melting point of salts (800–950 °C), and type II hot corrosion at a lower temperature, below the melting point (600–800 °C) [207,230]. These can be identified by the presence of the main corrosive salts Na_2SO_4 (MP 884 °C), NaCl (MP 801 °C) and V_2O_5 (MP 690 °C), which can form mixtures among themselves and with other elements [231–234].

Corrosion can also commonly occur due to the attack by molten silicates, especially the compound calcium–magnesium–alumino-silicate (CMAS). CMAS is composed of $\text{CaO-MgO-Al}_2\text{O}_3\text{-SiO}_2$ in varying proportions, depending on the environmental conditions [235]. CMAS can particularly affect aircraft turbines when flying at low altitudes and in arid areas. The compound forms from dust, sand, volcanic ash and industrial ash, and upon reaching temperatures above 1100–1200 °C in the propulsion system, it adheres to the turbine components, forming a glassy mass [236,237]. CMAS can interact with the TBC through two degradation mechanisms that can occur concurrently: (a) thermo-chemical impact, where CMAS dissolves the topcoat, leading to phase transformations, and (b) thermo-mechanical impact, where molten CMAS infiltrates deeply through the porous structure of the topcoat. As the temperature decreases to below the melting point of CMAS, the compound solidifies. Large differences in CTE and stiffness of the topcoat lead to premature failure [207,237–239].

7.6. Sintering of the TC

Sintering is an undesirable phenomenon in the case of TBCs, which, once it present, often leads to failure. It refers to the process in which TC particles agglomerate and adhere to each other during exposure to high temperatures, resulting in the formation of a dense and improper layer [240].

Excessive densification is highlighted by the reduction in the size of material porosities and micro-cracks and even the closure of extremely fine ones. This leads to the increased

elastic modulus and thermal conductivity of the TC, as there are fewer empty spaces to limit stiffness and heat flow [229].

In generic terms, a TBC is more long-lasting when it has lower values for these two parameters. The increase in stiffness results in increased stress due to the material shrinking, reduces strain tolerance and makes the TBC more susceptible to damage from FOD. Additionally, insulation is reduced due to increased thermal conductivity. All of these factors can result in early spallation [91,207,241–243].

The ceramic sinters at high temperatures, typically around $T^{\circ} = 0.5 \times T_m$ (T_m -melting temperature), but this phenomenon also depends on other parameters, such as exposure time and the composition of the TC [237]. To reduce the likelihood of sintering, practical measures include doping with elements such as La, Yb, Nd, Gd, Ti, etc. [244,245].

7.7. Creep and Rumpling

Creep is another phenomenon that can lead to the degradation of TBCs and represents continuous and progressive deformation of materials over time under mechanical and thermal loading, manifesting in all layers, but especially at the TC and TGO levels. Failure typically results in spallation. [246,247]. In general, creep occurs at $T^{\circ} = (0.4 - 0.5) \times T_m$ (T_m -melting temperature) [248]. Creep predominantly occurs in metals. The lower creep rate in ceramics is due to their reduced diffusion rate, requiring a higher activation energy compared to metals. The use of single-crystal alloys provides an advantage by eliminating grain boundaries, reducing the likelihood of deformation [249]. During creep deformation, the ceramic TBC does not deform plastically like metal, but rather through mechanisms of crack initiation and propagation, ultimately leading to failure typically manifested by spallation [248,250].

Rumpling (also known as *progressive roughness*, *undulation* or *ratcheting*) is another event that can lead to the degradation or failure of TBCs. Rumpling refers to the formation of wrinkles/waves on the surface of the TBC under the influence of high heat as a result of cyclic creep or cyclic oxidation [92,251,252]. It manifests especially at the BC level, which acquires a wavy shape induced further to the TGO and TC [253]. Rumpling occurs in the case of BCs made from MCrAlY and particularly in the case of aluminides of Ni and Pt (Ni,Pt)Al, with the observation that for the latter ones, there is a significant increase in TGO roughness due to excessive oxidation. This could lead to the detachment of the TC from the TGO [254]. The negative effects of rumpling are manifested by the appearance and propagation of cracks due to internal tensile stress at the peaks and compressive stress in the low areas, layer delamination and spallation [251,254,255]. The occurrence of rumpling depends especially on the heating cycle history, temperature intervals and the type and thickness of the TBC [255].

The manifestation of rumpling at the BC layer level is illustrated in Figure 8.

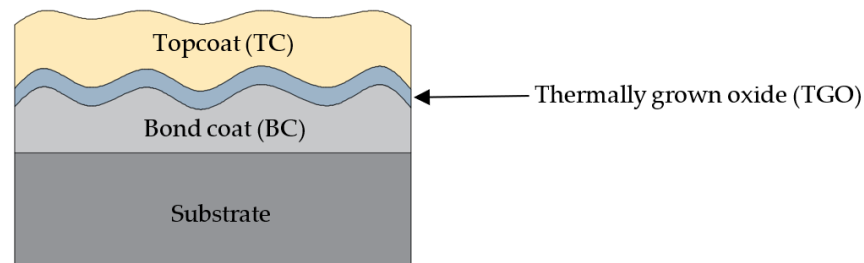


Figure 8. Rumpling at the BC layer level.

8. Study Perspectives

As for promising research directions, coatings for the fifth and sixth generation of superalloys present a path worth exploring to increase the operating temperatures of components, as there is an ambition to surpass operating temperatures of 1700 °C in turbines.

Additionally, the development of simple rare earth combinations, but with structures incorporating charge disorder and bond fluctuation, may exhibit performance that equals or surpasses high-entropy materials with a large number of elements in their composition.

Depending on the application domains and working conditions, the elements coated with TBCs may store a certain amount of residual stress. Practical studies on the formation and influence of this phenomenon on failure should be approached in a manner that provides measured results following experimental conditions. Additionally, experimental studies on stress relief methods originating from the science of heat treatments can be investigated.

Delving into the nanometric or atomic scale to study how thermal vibrations travel through the ceramic coating layer and its interface with the metallic substrate can lead to advancements in minimizing heat transfer and managing thermal expansions.

9. Conclusions

This review provides a comprehensive analysis of TBCs applied to metallic materials, offering insights into their structure, role, various materials, coating processes, durability mechanisms and failure processes. It is important to note that this paper does not cover all aspects related to TBCs due to the broad subject matter. Instead, it examines the challenges and opportunities involved in the evolution of thermal protective coatings, exploring various structural and compositional dimensions. This paper condenses a structured collection of information representing a relevant document for the current state of TBCs.

Following the review of the literature, several key insights and areas of interest have emerged in the field of coatings. TBCs play a pivotal role in protecting metal components exposed to extreme thermal conditions in harmful working environments, such as in the aerospace industry, energy generation and the automotive and maritime sectors. The classic double-layer coating consisting of a BC and a ceramic TC remains a focal point with diversification in doping possibilities using rare earth combinations, which, in some applications, can match the performance of high-entropy coatings and multi-layer coatings. Coating methods such as APS, EB-PVD and SPS remain highly relevant, with them being the most widely used techniques.

Author Contributions: Conceptualization, M.B.; methodology, M.B.; formal analysis, M.B. and I.P.; investigation, M.B.; resources, M.B.; data curation, M.B.; writing—original draft preparation, M.B.; writing—review and editing, M.B. and I.P.; visualization, M.B.; supervision, I.P.; project administration, not applicable; funding acquisition, not applicable. All authors have read and agreed to the published version of the manuscript.

Funding: This research received no external funding.

Data Availability Statement: Not applicable.

Acknowledgments: The authors would like to express their sincere appreciation to the contributors whose photographs, sourced from the copyright-free website <https://pixabay.com>, have been utilized to illustrate the main application areas of TBCs (Section 3, Figure 2). Despite their copyright-free status, we believe it is important to credit their contributions to this work, as follows: a. Aerospace applications—dayamay; b. Power generation—grunzibaer; c. Automotive applications—andreas160578; d. Naval industry—zzkonst.

Conflicts of Interest: The authors declare no conflicts of interest.

References

1. Simic, M.; Alil, A.; Martinović, S.; Vlahović, M.; Savić, A.; Volkov-Husović, T. High temperature materials: Properties, demands and applications. *Hem. Ind.* **2020**, *74*, 273–284. [[CrossRef](#)]
2. Chellaganesh, D.; Adam Khan, M.; Winowlin Jappes, J.T. Thermal barrier coatings for high temperature applications—A short review. *Mater. Today Proc.* **2021**, *45*, 1529–1534. [[CrossRef](#)]
3. Song, J.; Wang, L.; Yao, J.; Dong, H. Multi-Scale Structural Design and Advanced Materials for Thermal Barrier Coatings with High Thermal Insulation: A Review. *Coatings* **2023**, *13*, 343. [[CrossRef](#)]

4. Harrison, W.N.; Moore, D.G.; Richmond, J.C. *Review of an Investigation of Ceramic Coatings for Metallic Turbine Parts and Other High-Temperature Applications*; TN-1186; National Advisory Committee for Aeronautics: Washington, DC, USA, 1947.
5. Garrett, F.B.; Gyorgak, C.A. *Adhesive and Protective Characteristics of Ceramic Coating A-417 and Its Effect on Engine Life of Forged Refractory-26 (AMS 5760) and Cast Stellite (AMS 5385) Turbine Blades*; RM-E52L30; National Advisory Committee for Aeronautics: Washington, DC, USA, 1953.
6. Shafer, L.J.; Stepka, F.S.; Brown, W.B. *Comparison of Theoretically and Experimentally Determined Effects of Oxide Coatings Supplied by Fuel Additives on Uncooled Turbine-Blade Temperature during Transient Turbojet-Engine Operation*; RM-E53A19; National Advisory Committee for Aeronautics: Washington, DC, USA, 1953.
7. Miller, R.A. Current status of thermal barrier coatings—An overview. *Surf. Coat. Technol.* **1987**, *30*, 1–11. [[CrossRef](#)]
8. Miller, R.A. Thermal barrier coatings for aircraft engines: History and directions. *J. Therm. Spray Technol.* **1997**, *6*, 35–42. [[CrossRef](#)]
9. Miller, R.A. History of Thermal Barrier Coatings for Gas Turbine Engines: Emphasizing NASA's Role from 1942 to 1990. In *Proceedings of the Thermal Barrier Coatings II, Engineering Conference International* (No. NASA/TM-2009-215459), Klostersee, Germany, 12–17 August 2007.
10. Clarke, D.R.; Oechsner, M.; Padture, N.P. Thermal-barrier coatings for more efficient gas-turbine engines. *MRS Bull.* **2012**, *37*, 891–898. [[CrossRef](#)]
11. Barwinska, I.; Kopec, M.; Kukla, D.; Senderowski, C.; Kowalewski, Z.L. Thermal Barrier Coatings for High-Temperature Performance of Nickel-Based Superalloys: A Synthetic Review. *Coatings* **2023**, *13*, 769. [[CrossRef](#)]
12. Sezavar, A.; Sajjadi, S.A.; Babakhani, A.; Peng, R.L.; Yuan, K. Hot Corrosion Behavior of Micro- and Nanostructured Thermal Barrier Coatings: Conventional Bilayer and Compositionally Graded Layer YSZ. *Oxid. Met.* **2021**, *96*, 469–486. [[CrossRef](#)]
13. Patnaik, P.C.; Huang, X.; Singh, J. State of the Art and Future Trends in the Development of Thermal Barrier Coating Systems. In *Innovative Missile Systems; Meeting Proceedings RTO-MP-AVT-135*; RTO: Neuilly-sur-Seine, France, 2006; pp. 38:1–38:20.
14. Krishna, V.G.; Parammasivam, K.M. Thermal barrier coated surface modifications for gas turbine film cooling: A review. *J. Therm. Anal. Calorim.* **2021**, *146*, 545–580. [[CrossRef](#)]
15. Fiedler, T.; Rösler, J.; Bäker, M.; Hötte, F.; von Sethe, C.; Daub, D.; Haupt, M.; Haidn, O.J.; Esser, B.; Gülhan, A. Mechanical Integrity of Thermal Barrier Coatings: Coating Development and Micromechanics. In *Future Space-Transport-System Components under High Thermal and Mechanical Loads*; Springer: Berlin/Heidelberg, Germany, 2021; Volume 146, pp. 295–307. [[CrossRef](#)]
16. Fiedler, T.; Schloesser, J.; Rösler, J. Development of a thermal-barrier coating-system for rocket combustion chambers. In *Proceedings of the 6th European Conference for Aerospace Sciences*, Kraków, Poland, 29 June–3 July 2015.
17. Greuel, D.; Suslov, D.; Haidn, O.; Fritscher, K. Thermal Barrier Coatings for Cryogenic Rocket Engines. In *Proceedings of the 38th AIAA/ASME/SAE/ASEE/JPC Conference and Exhibit*, Indianapolis, IN, USA, 7–10 July 2002; p. 4145.
18. Liu, L.; Yu, H.; Zheng, C.; Ye, D.; He, W.; Wang, S.; Li, J.; Wu, L.; Zhang, Y.; Xie, J.; et al. Nondestructive Thickness Measurement of Thermal Barrier Coatings for Turbine Blades by Terahertz Time Domain Spectroscopy. *Photonics* **2023**, *10*, 105. [[CrossRef](#)]
19. Biswas, S.; Ramachandra, S.; Hans, P.; Kumar, S.S.P. Materials for Gas Turbine Engines: Present Status, Future Trends and Indigenous Efforts. *J. Indian Inst. Sci.* **2022**, *102*, 297–309. [[CrossRef](#)]
20. ASM Aerospace Specification Metals. Available online: <https://asm.matweb.com> (accessed on 5 March 2024).
21. Zhang, Y.; Liu, P.; Li, Z. Impact of Cooling with Thermal Barrier Coatings on Flow Passage in a Gas Turbine. *Energies* **2022**, *15*, 85. [[CrossRef](#)]
22. Kistenmacher, D.A.; Davidson, F.T.; Bogard, D.G. Realistic Trench Film Cooling With a Thermal Barrier Coating and Deposition. In *Proceedings of the ASME Turbo Expo 2013: Turbine Technical Conference and Exposition*, Volume 3B: Heat Transfer, San Antonio, TX, USA, 3–7 June 2013; p. V03BT13A057. [[CrossRef](#)]
23. Davidson, F.T.; Kistenmacher, D.A.; Bogard, D.G. Film Cooling With a Thermal Barrier Coating: Round Holes, Craters, and Trenches. *J. Turbomach.* **2014**, *136*, 041007. [[CrossRef](#)]
24. Ghosh, S.; Saha, M.; Bakshi, S.; Mondal, S. Effect of Thermal Barrier Coating in Sustainable Power production of Gas Turbines. *IOP Conf. Ser. Mater. Sci. Eng.* **2021**, *1187*, 012034. [[CrossRef](#)]
25. Ali, Z.A.; Mohammad, T.R. Effects of Thermal Barrier coating (TBC) thickness on temperature distribution of gas turbine blade. In *Proceedings of the 3rd Conference on Advances in Mechanical Engineering*, Istanbul, Turkey, 19–21 December 2017.
26. Yang, X.; Zhang, J.; Lu, Z.; Park, H.Y.; Jung, Y.G.; Park, H.; Koo, D.D.; Sinatra, R.; Zhang, J. Removal and repair techniques for thermal barrier coatings: A review. *Trans. IMF* **2020**, *98*, 121–128. [[CrossRef](#)]
27. Al-Shami, M.; Mohamed, O.; Abu Elhaija, W. Energy-Efficient Control of a Gas Turbine Power Generation System. *Designs* **2023**, *7*, 85. [[CrossRef](#)]
28. Khattak, M.A.; Mohd Ali, N.S.; Abidin, N.H.Z.; Azhar, N.S.; Omar, M.H. Common Type of Turbines in Power Plant: A Review. *J. Adv. Res. Appl. Sci. Eng. Technol.* **2016**, *3*, 77–100.
29. Slade, S.; Palmer, C. Worldwide Gas Turbine Forecast. In *Turbomachinery International Handbook*; Turbomachinery International: Norwalk, CT, USA, 2019; Volume 59, pp. 34–39.
30. Slade, S.; Palmer, C. Worldwide Market Report: 2020 proved to be an interesting year for gas turbines. In *Turbomachinery International Handbook*; Turbomachinery International: Norwalk, CT, USA, 2020; Volume 60, pp. 28–29.
31. Rao, A. Advanced Brayton Cycles. In *The Gas Turbine Handbook*; U.S. Department of Energy-National Energy Technology Laboratory: Morgantown, WV, USA, 2006; pp. 115–121.

32. Pirin, O.T.; Jardón, E.R.; García, J.C.; Mariaca, Y.; Hernández, Y.S.; Ñeco, R.; Dávalos, O. Effect of Thermal Barrier Coating on the Thermal Stress of Gas Microturbine Blades and Nozzles. *J. Mech. Eng.* **2020**, *66*, 581–590. [CrossRef]
33. Jude, S.A.A.; Winowlin Jappes, J.T.; Adamkhan, M. Thermal barrier coatings for high-temperature application on superalloy substrates—A review. *Mater. Today Proc.* **2022**, *60*, 1670–1675. [CrossRef]
34. Safakish, G.R. Temperature Estimation in the Combustion Chamber of an Internal Combustion Engine. *Adv. Mech. Eng.* **2012**, *4*, 931584. [CrossRef]
35. Naval Education and Training Professional Development and Technology Center. *Construction Mechanic Basic. Volume 1*; NAVEDTRA 14264; Naval Education and Training Professional Development and Technology Center: Pensacola, FL, USA, 1998.
36. Hayes, T.K.; White, R.A.; Peters, J.E. *Combustion Chamber Temperature and Instantaneous Local Heat Flux Measurements in a Spark Ignition Engine*; SAE Technical Paper No. 930217; SAE International: Warrendale, PA, USA, 1993. [CrossRef]
37. Sharma, P.; Dwivedi, V.K.; Kumar, D. A Review on Thermal Barrier Coatings (TBC) Usage and Effect on Internal Combustion Engine. In *Advances in Fluid and Thermal Engineering*; Springer: Singapore, 2021; pp. 77–85. [CrossRef]
38. Dahham, R.Y.; Wei, H.; Pan, J. Improving Thermal Efficiency of Internal Combustion Engines: Recent Progress and Remaining Challenges. *Energies* **2022**, *15*, 6222. [CrossRef]
39. Rohini, A.; Prema, S. A review on thermal barrier coating for diesel engine and its characteristics studies. *J. Phys. Conf. Ser.* **2020**, *1473*, 012039. [CrossRef]
40. Liu, Y.; Lei, J.; Deng, X.; Liu, Y.; Sun, D.; Zhang, Y. Research and analysis of a thermal optimisation design method for aluminium alloy pistons in diesel engines. *Case Stud. Therm. Eng.* **2023**, *52*, 103667. [CrossRef]
41. Das, D.; Majumdar, G.; Sen, R.S.; Ghosh, B.B. The Effects of Thermal Barrier Coatings on Diesel Engine Performance and Emission. *J. Inst. Eng. India Ser. C* **2014**, *95*, 63–68. [CrossRef]
42. Raghu; Girishkumar, G.S.; Chandrashekar, K. Experimental Study of the Effect of Thermal Barrier Coating on Diesel Engine Performance. *Int. Res. J. Eng. Technol.* **2018**, *5*, 2051–2054.
43. Karthickeyan, V.; Balamurugan, P. Effect of thermal barrier coating with various blends of pumpkin seed oil methyl ester in DI diesel engine. *Heat Mass Transf.* **2017**, *53*, 3141–3154. [CrossRef]
44. Uchida, N. A review of thermal barrier coatings for improvement in thermal efficiency of both gasoline and diesel reciprocating engines. *Int. J. Engine Res.* **2022**, *23*, 3–19. [CrossRef]
45. Durat, M.; Kapsiz, M.; Nart, E.; Ficici, F.; Parlak, A. The effects of coating materials in spark ignition engine design. *Mater. Des.* **2012**, *36*, 540–545. [CrossRef]
46. Liu, H.; Hong, Q.; Liu, H.; Huang, Z.; Zhang, X.; Chen, W.; Zeng, X.; Pan, S. Effects of Temperature and Additives on NOx Emission From Combustion of Fast-Growing Grass. *Front. Energy Res.* **2021**, *9*, 772755. [CrossRef]
47. Bussman, W.R.; Baukal, C.E. Ambient conditions impact CO and NOx emissions: Part II. *Pet. Technol. Q.* **2009**, *14*, 37–41.
48. Sehili, Y.; Loubar, K.; Lounici, M.S.; Tarabet, L.; Cerdoun, M.; Lacroix, C. Development of knock prediction technique in dual fuel engines and its mitigation with direct water injection. *Fuel* **2024**, *358*, 130297. [CrossRef]
49. Kawaguchi, A.; Wakisaka, Y.; Nishikawa, N.; Kosaka, H.; Yamashita, H.; Yamashita, C.; Iguma, H.; Fukui, K.; Takada, N.; Tomoda, T. Thermo-swing insulation to reduce heat loss from the combustion chamber wall of a diesel engine. *Int. J. Engine Res.* **2019**, *20*, 805–816. [CrossRef]
50. MAN Energy Solutions. Basic Principles of Ship Propulsion. Available online: <https://www.man-es.com> (accessed on 6 March 2024).
51. Jin, Z.; Yang, Y. Research on ship electric propulsion. *IOP Conf. Ser. Earth Environ. Sci.* **2020**, *446*, 042057. [CrossRef]
52. Ozgurluk, Y.; Doleker, K.M.; Karaoglanli, A.C. Hot corrosion behavior of YSZ, Gd₂Zr₂O₇ and YSZ/Gd₂Zr₂O₇ thermal barrier coatings exposed to molten sulfate and vanadate salt. *Appl. Surf. Sci.* **2018**, *438*, 96–113. [CrossRef]
53. Parthiban, K.; Roy, P.; Ghosh, S. Hot Corrosion Behaviour of Three-Layered Functionally Graded Glass–ceramic–YSZ-based Thermal Barrier Coating System. *Trans. Indian Inst. Met.* **2023**, *77*, 1407–1412. [CrossRef]
54. Wu, S.; Zhao, Y.; Li, W.; Liu, W.; Wu, Y.; Zhao, Z. Na₂SO₄ + NaCl molten salts corrosion mechanism of thermal barrier coatings used in ships. *J. Therm. Anal. Calorim.* **2021**, *144*, 2043–2056. [CrossRef]
55. Hille, T.; Suiker, A.A.; Turteltaub, S.R. Engineering Fracture Mechanics. Microcrack nucleation in thermal barrier coating systems. *Eng. Fract. Mech.* **2009**, *76*, 813–825. [CrossRef]
56. Li, B.; Fan, X.; Li, D.; Jiang, P. Design of Thermal Barrier Coatings Thickness for Gas Turbine Blade Based on Finite Element Analysis. *Math. Probl. Eng.* **2017**, *2017*, 2147830. [CrossRef]
57. Mouritz, A.P. Superalloys for gas turbine engines. In *Introduction to Aerospace Materials*; Woodhead Publishing Limited: Sawston, UK, 2012; pp. 251–267.
58. Gurrappa, I.; Yashwanth, I.V.S. The Importance of Corrosion and the Necessity of Applying Intelligent Coatings for Its Control. In *Intelligent Coatings for Corrosion Control*; Butterworth-Heinemann: Oxford, UK, 2015; pp. 17–58. [CrossRef]
59. Mukherji, D.; Rösler, J.; Strunz, P.; Gilles, R.; Schumacher, G.; Piegert, S. Beyond Ni-based superalloys: Development of CoRe-based alloys for gas turbine applications at very high temperatures. *Int. J. Mater. Res.* **2011**, *102*, 1125–1132. [CrossRef]
60. Nowotnik, A. Nickel-Based Superalloys. In *Reference Module in Materials Science and Materials Engineering*; Elsevier: Amsterdam, The Netherlands, 2017. [CrossRef]
61. Yu, J.; Wang, D.; Chen, J.; Yang, C.; Hao, X.; Zhou, J.; Li, D.; Shu, D.; Xiao, C.; Peng, Y. High Temperature Behaviors of a Casting Nickel-Based Superalloy Used for 815 °C. *Materials* **2021**, *14*, 716. [CrossRef]

62. Horke, K.; Meyer, A.; Singer, R.F. Metal injection molding (MIM) of nickel-base superalloys. In *Handbook of Metal Injection Molding*, 2nd ed.; Woodhead Publishing: Sawston, UK, 2019; pp. 575–608. [[CrossRef](#)]
63. Reed, R.C. *The Superalloys. Fundamentals and Applications*; Cambridge University Press: Cambridge, UK, 2006; pp. 1–28.
64. Wee, S.; Do, J.; Kim, K.; Lee, C.; Seok, C.; Choi, B.G.; Choi, Y.; Kim, W. Review on Mechanical Thermal Properties of Superalloys and Thermal Barrier Coating Used in Gas Turbines. *Appl. Sci.* **2020**, *10*, 5476. [[CrossRef](#)]
65. Kawagishi, K.; Yeh, A.; Yokokawa, T.; Kobayashi, T.; Koizumi, Y.; Harada, H. Development of an Oxidation-Resistant High-Strength Sixth-Generation Single-Crystal Superalloy TMS-238. *Superalloys* **2012**, *9*, 189–195. [[CrossRef](#)]
66. Jithin, S.D.; Senthil, K.S.; Vijay Vishal, K.E.; Sundaramali, G. Comparative Analysis between 5th and 6th Generation Superalloys and Previous Generation Superalloys. *Adv. Mater. Sci. Eng.* **2022**, *2022*, 3530689. [[CrossRef](#)]
67. Saltykov, P.; Fabrichnaya, O.; Golczewski, J.; Aldinger, F. Thermodynamic modeling of oxidation of Al–Cr–Ni alloys. *J. Alloys Compd.* **2004**, *381*, 99–113. [[CrossRef](#)]
68. Aabid, A.; Khan, S.A. Optimization of Heat Transfer on Thermal Barrier Coated Gas Turbine Blade. *IOP Conf. Ser. Mater. Sci. Eng.* **2018**, *370*, 012022. [[CrossRef](#)]
69. Haynes, J.A.; Ferber, M.K.; Porter, W.D. Thermal cycling behavior of plasma-sprayed thermal barrier coatings with various MCrAlX bond coats. *J. Therm. Spray Technol.* **2000**, *9*, 38–48. [[CrossRef](#)]
70. Cojocar, C.V.; Aghasibeig, M.; Irissou, E. NiCoCrAlX (X = Y, Hf and Si) Bond Coats by Cold Spray for High Temperature Applications. *J. Therm. Spray Technol.* **2022**, *31*, 176–185. [[CrossRef](#)] [[PubMed](#)]
71. Kang, Y. Oxidation and Corrosion of New MCrAlX Coatings-Modelling and Experiments. Doctoral Thesis, Linköping University, Linköping, Sweden, 2014. ISBN 978-91-7519-247-5.
72. Nicholls, J.R. Designing oxidation-resistant coatings. *JOM* **2000**, *52*, 28–35. [[CrossRef](#)]
73. Abedi, H.R.; Salehi, M.; Shafyei, A. Mechanical and Thermal Properties of Double-layer and Triple-layer Thermal Barrier Coatings with Different Ceramic Top Coats onto Polyimide Matrix Composite. *Ceram. Int.* **2017**, *43*, 12770–12780. [[CrossRef](#)]
74. Naumenko, D.; Shemet, V.; Singheiser, L.; Quadackers, W.J. Failure mechanisms of thermal barrier coatings on MCrAlY-type bondcoats associated with the formation of the thermally grown oxide. *J. Mater. Sci.* **2009**, *44*, 1687–1703. [[CrossRef](#)]
75. Naumenko, D.; Pillai, R.; Chyrkin, A.; Quadackers, W.J. Overview on Recent Developments of Bondcoats for Plasma-Sprayed Thermal Barrier Coatings. *J. Therm. Spray Technol.* **2017**, *26*, 1743–1757. [[CrossRef](#)]
76. Ogawa, K.; Ito, K.; Shoji, T.; Seo, D.W.; Tezuka, H.; Kato, H. Effects of Ce and Si additions to CoNiCrAlY bond coat materials on oxidation behavior and crack propagation of thermal barrier coatings. *J. Therm. Spray Technol.* **2006**, *15*, 640–651. [[CrossRef](#)]
77. Duan, W.; Li, Y.; Qiang, W. Effect of Hf-Doped MCrAlY Alloy on the Structure and Properties of Thermally Grown Oxide Layer. *J. Mater. Eng. Perform.* **2023**; in press. [[CrossRef](#)]
78. Duan, W.; Huang, B.; Li, Y.; Huang, X.; Zhou, M.; Qiang, W. Hf and Ta co-doping MCrAlY alloy to improve the lifetime of coatings. *Surf. Coat. Technol.* **2023**, *468*, 129781. [[CrossRef](#)]
79. Wang, H.X.; Zhang, Y.; Cheng, J.L.; Li, Y.S. High temperature oxidation resistance and microstructure change of aluminized coating on copper substrate. *Trans. Nonferrous Met. Soc. China* **2015**, *25*, 184–190. [[CrossRef](#)]
80. Song, P. Influence of Material and Testing Parameters on the Lifetime of TBC Systems with MCrAlY and NiPtAl Bondcoats. Doctoral Thesis, RWTH Aachen University, Aachen, Germany, 2011. ISBN 978-3-89336-783-2.
81. Marino, K.A.; Hinnemann, B.; Carter, E.A. Atomic-scale insight and design principles for turbine engine thermal barrier coatings from theory. *Proc. Natl. Acad. Sci. USA* **2011**, *108*, 5480–5487. [[CrossRef](#)]
82. Zhou, C.G.; Song, Y.X. Oxidation and hot corrosion of thermal barrier coatings (TBCs). In *Thermal Barrier Coatings*; Woodhead Publishing: Sawston, UK, 2011; pp. 193–214. [[CrossRef](#)]
83. Soare, A.; Csáki, I.; Sohaci, M.; Oprea, C.; Soare, S.; Costina, I.; Petrescu, M.I. New Bond Coat Materials for Thermal Barrier Coating Systems Processed Via Different Routes. *IOP Conf. Ser. Mater. Sci. Eng.* **2017**, *209*, 012045. [[CrossRef](#)]
84. Li, S.; Qi, H.; Song, J.; Yang, X.; Che, C. Effect of bond-coat surface roughness on failure mechanism and lifetime of air plasma spraying thermal barrier coatings. *Sci. China Technol. Sci.* **2019**, *62*, 989–995. [[CrossRef](#)]
85. Xie, Z.; Liu, Q.; Lee, K.I.; Zhu, W.; Wu, L.T.; Wu, R.T. The Effect of Bond Coat Roughness on the CMAS Hot Corrosion Resistance of EB-PVD Thermal Barrier Coatings. *Coatings* **2022**, *12*, 596. [[CrossRef](#)]
86. Takahashi, R.J.; Assis, J.M.K.; Neto, F.P.; Reis, D.A.P. Heat treatment for TGO growth on NiCrAlY for TBC application. *Mater. Res. Express* **2019**, *6*, 126442. [[CrossRef](#)]
87. Wei, Z.; Liu, Y.; Cheng, B.; Tahir, A. Influence of non-uniform feature of thermally grown oxide thickness on the local stress state and cracking behavior in TBC. *Surf. Coat. Technol.* **2022**, *443*, 128607. [[CrossRef](#)]
88. Liu, C. Study of Bond Coats and Failure Mechanisms of Thermal Barrier Coatings. Doctoral Thesis, University of Manchester, Manchester, UK, 2019.
89. Chen, W.R.; Wu, X.; Marple, B.R.; Nagy, D.R.; Patnaik, P.C. TGO growth behaviour in TBCs with APS and HVOF bond coats. *Surf. Coat. Technol.* **2008**, *202*, 2677–2683. [[CrossRef](#)]
90. Garcia-Herrera, J.E.; Espinosa-Arbeláez, D.G.; Cáceres-Díaz, L.A.; Mondragón-Rodríguez, G.C.; Ruiz-Luna, H.; González-Hernández, J.; Trápaga-Martínez, L.G.; Muñoz-Saldaña, J.; Alvarado-Orozco, J.M. Effect of pre-oxidation treatments on the structural, microstructural, and chemical properties of β -(Ni,Pt)Al system. *Surf. Coat. Technol.* **2019**, *367*, 156–164. [[CrossRef](#)]
91. Hille, T.S. Lifetime Modeling Thermal Barrier Coatings. Doctoral Thesis, Universität Stuttgart, Stuttgart, Germany, 2009. ISBN 978-90-771-7243-8.

92. Padture, N.P.; Gell, M.; Jordan, E.H. TBCs for Gas-Turbine Engine Applications. *Science* **2002**, *296*, 280–284. [CrossRef]
93. Moskal, G. Thermal barrier coatings: Characteristics of microstructure and properties, generation and directions of development of bond. *J. Achiev. Mater. Manuf. Eng.* **2009**, *37*, 323–331.
94. Zhu, D.; Miller, R.A. Development of Advanced Low Conductivity Thermal Barrier Coatings. *Int. J. Appl. Ceram. Technol.* **2004**, *1*, 86–94. [CrossRef]
95. Ma, W.; Jarligo, M.; Mack, D.E.; Pitzer, D.; Malzbender, J.; Vaßen, R.; Stöver, D. New Generation Perovskite Thermal Barrier Coating Materials. *J. Therm. Spray Technol.* **2008**, *17*, 831–837. [CrossRef]
96. Mebdoua-Lahmar, Y.; Derbal-Habak, H.; Benkhaled, A. Alternative Materials for Performant TBCs: Short Review. *J. Minera Land Mater. Sci.* **2023**, *4*, 1051. [CrossRef]
97. Vaßen, R.; Jarligo, M.O.; Steinke, T.; Mack, D.E.; Stöver, D. Overview on advanced thermal barrier coatings. *Surf. Coat. Technol.* **2010**, *205*, 938–942. [CrossRef]
98. Shvydyuk, K.O.; Nunes-Pereira, J.; Rodrigues, F.F.; Silva, A.P. Review of Ceramic Composites in Aeronautics and Aerospace: A Multifunctional Approach for TPS, TBC and DBD Applications. *Ceramics* **2023**, *6*, 195–230. [CrossRef]
99. Liu, L.; Wang, S.; Zhang, B.; Jiang, G.; Liu, H.; Yang, J.; Wang, J.; Liu, W. Present status and prospects of nanostructured thermal barrier coatings and their performance improvement strategies: A review. *J. Manuf. Processes* **2023**, *97*, 12–34. [CrossRef]
100. Cao, X.Q.; Vassen, R.; Stoeber, D. Ceramic materials for thermal barrier coatings. *J. Eur. Ceram. Soc.* **2004**, *24*, 1–10. [CrossRef]
101. Naraparaju, R.; Pubbysetty, R.P.; Mechnich, P.; Schulz, U. EB-PVD alumina (Al_2O_3) as a top coat on 7YSZ TBCs against CMAS/VA infiltration: Deposition and reaction mechanisms. *J. Eur. Ceram. Soc.* **2018**, *38*, 3333–3346. [CrossRef]
102. Bolelli, G.; Meschini, D.; Varis, T.; Testa, V.; Morelli, S.; Lusvardi, L.; Vuoristo, P. Corrosion Properties of Thermally Sprayed Bond Coatings Under Plasma-Sprayed Chromia Coating in Sulfuric Acid Solutions. *J. Therm. Spray Technol.* **2020**, *29*, 270–284. [CrossRef]
103. Venkadesan, G.; Muthusamy, J. Experimental investigation of Al_2O_3 /8YSZ and CeO_2 /8YSZ plasma sprayed thermal barrier coating on diesel engine. *Ceram. Int.* **2019**, *45*, 3166–3176. [CrossRef]
104. Kiryc, M.; Kazamer, N.; Kurumlu, D.; Marginean, G. Comparative Study on the Thermal Performance of Cr-Cr_xO_y and YSZ-CoNiCrAlY Coatings Exposed at 900 °C. *Materials* **2021**, *14*, 6040. [CrossRef] [PubMed]
105. Iqbal, A.; Moskal, G. Recent Development in Advance Ceramic Materials and Understanding the Mechanisms of Thermal Barrier Coatings Degradation. *Arch. Comput. Methods Eng.* **2023**, *30*, 4855–4896. [CrossRef]
106. Clarke, D.R.; Levi, C.G. Materials Design for The Next Generation Thermal Barrier Coatings. *Annu. Rev. Mater. Res.* **2003**, *33*, 383–417. [CrossRef]
107. Song, X.; Ding, Y.; Zhang, J.; Jiang, C.; Liu, Z.; Lin, C.; Zheng, W.; Zeng, Y. Thermophysical and mechanical properties of cubic, tetragonal and monoclinic ZrO_2 . *J. Mater. Res. Technol.* **2023**, *23*, 648–655. [CrossRef]
108. Yu, Z.; Qi, T.; Ge, M.; Zhang, W.; Hu, Z.; Sun, X. Microstructures and phase compositions of Y_2O_3 - ZrO_2 - HfO_2 solid solutions. *Ceram. Int.* **2023**, *49*, 26119–26128. [CrossRef]
109. Esmaeilkhani, A.H.; Sharifianjazi, F.; Ahmadi, E.; Ijadi, A.; Meskher, H.; Zarei, R.; Nili-Ahmadabadi, M.; Irandoost, M.; Karimi, N.; Ghiasvand, A. Thermal barrier coating with improved durability: An overview of doped, nanostructured, multilayered, and gradient-structured zirconia-based thermal barrier coatings. *Mater. Today Commun.* **2023**, *37*, 107514. [CrossRef]
110. Fabris, S.; Paxton, A.T.; Finnis, M.W. A stabilization mechanism of zirconia based on oxygen vacancies only. *Acta Mater.* **2002**, *50*, 5171–5178. [CrossRef]
111. Smialek, J.; Miller, R. Revisiting the Birth of 7YSZ Thermal Barrier Coatings: Stephan Stecura. *Coatings* **2018**, *8*, 255. [CrossRef]
112. MatWeb. Yttria Stabilized Zirconia, YSZ. Available online: <https://www.matweb.com> (accessed on 10 March 2024).
113. Vaßen, R.; Mack, D.E.; Tandler, M.; Sohn, Y.J.; Sebold, D.; Guillon, O. Unique performance of thermal barrier coatings made of yttria-stabilized zirconia at extreme temperatures (>1500 °C). *J. Am. Ceram. Soc.* **2020**, *104*, 463–471. [CrossRef]
114. Chee Hon Cheong, A.; Sivanesan, S. Perspective Chapter: The Application of Yttria-Stabilized Zirconia (YSZ). In *Zirconia—New Advances, Structure, Fabrication and Applications*; IntechOpen: London, UK, 2023. [CrossRef]
115. Borik, M.A.; Kulebyakin, A.V.; Lomonova, E.E.; Milovich, F.O.; Myzina, V.A.; Ryabochkina, P.A.; Tabachkova, N.Y.; Sidorova, N.V.; Chislov, A.S. Partially Yttria-Stabilized Zirconia Crystals Co-Doped with Neodymium, Cerium, Terbium, Erbium or Ytterbium Oxides. *Crystals* **2021**, *11*, 1587. [CrossRef]
116. Yang, M.; Zhu, Y.; Wang, X.; Wang, Q.; Ai, L.; Zhao, L.; Chu, Y.; Guo, S.; Hu, J.; Zhang, Q. Preparation and thermophysical properties of Ti⁴⁺ doped zirconia matrix thermal barrier coatings. *J. Alloys Compd.* **2019**, *777*, 646–654. [CrossRef]
117. Tian, Y.; Liu, S.; Zhang, X.; Xiao, S.; Sun, J.; Zhang, J.; Han, G. Controlled synthesis of Bi_2O_3 -YSZ composite powders and their sintering behavior for high-performance electrolytes. *Int. J. Appl. Ceram. Technol.* **2023**, *20*, 1398–1407. [CrossRef]
118. Xing, Y.Z.; Men, Y.N.; Feng, X.; Geng, J.H.; Zou, Z.R.; Chen, F.H. Evolutions in the microstructure and ionic conductivity of CuO-doped yttria-stabilized zirconia. *J. Solid State Chem.* **2022**, *315*, 123497. [CrossRef]
119. Pollet, M.; Marinell, S.; Desgardin, G. CaZrO_3 , a Ni-co-sinterable dielectric material for base metal-multilayer ceramic capacitor applications. *J. Eur. Ceram. Soc.* **2004**, *24*, 119–127. [CrossRef]
120. Garcia, E.; Cano, C.; Osendi, M.I.; Miranzo, P.; Coyle, T.W. Thermal Behaviour of Thermally Sprayed CaZrO_3 Coatings. In *Thermal Spray. In Proceedings of the International Thermal Spray Conference, Maastricht, The Netherlands, 2–4 June 2008*; pp. 1004–1008. [CrossRef]

121. Ejaz, N.; Ali, L.; Ahmad, A.; Mansoor, M.; Asim, M.M.; Rauf, A.; Mehmood, K. Thermo-Physical Properties Measurement of Advanced TBC Materials with Pyrochlore and Perovskite Structures. *Key Eng. Mater.* **2018**, *778*, 236–244. [[CrossRef](#)]
122. Kumar, V.; Sharma, R.; Sharma, A.K.; Sharma, R.K. Mechanical stresses analysis of a partially ceramic coated cylinder liners using finite element analysis. *Mater. Today Proc.* **2023**, *72*, 2369–2377. [[CrossRef](#)]
123. Drazin, J.W.; Castro, R.H.R. Phase Stability in Calcia-Doped Zirconia Nanocrystals. *J. Am. Ceram. Soc.* **2016**, *99*, 1778–1785. [[CrossRef](#)]
124. Oerlikon. Material Product Data Sheet. Magnesia-Stabilized Zirconium Oxide Powders. Available online: <https://www.oerlikon.com> (accessed on 10 March 2024).
125. STC Material Solutions. Material Product Data Sheet. Magnesia Stabilized Zirconia (MSZ). Available online: <https://ceramics.net> (accessed on 10 March 2024).
126. Fouad, M.G.; Ghazaly, N.M.; Abd El Tawwab, A.M.; Abd El Gwwad, K.A. Finite Element Thermal Analysis of A Ceramic Coated Si Engine Piston Considering Coating Thickness. *Am. J. Eng. Res.* **2017**, *6*, 109–113.
127. Azhar, A.Z.A.; Mohamad, H.; Ratnam, M.M.; Ahmad, Z.A. The effects of MgO addition on microstructure, mechanical properties and wear performance of zirconia-toughened alumina cutting inserts. *J. Alloys Compd.* **2010**, *497*, 316–320. [[CrossRef](#)]
128. Yamagata, C.; Mello-Castanho, S.R.H.; Paschoal, J.O.A. Synthesis and Mechanical Properties of Stabilized Zirconia Ceramics: MgO–ZrO₂ and Y₂O₃–MgO–ZrO₂. In Proceedings of the Congresso Brasileiro de Engenharia e Ciência dos Materiais, Cuiaba, MT, Brazil, 9–13 November 2014.
129. Gul, S.R.; Khan, M.; Zeng, Y.; Wu, B. Understanding the thermodynamic properties of 20% CeO₂ stabilized ZrO₂ coatings with atomistic modeling and simulations. *Mater. Res. Express* **2019**, *6*, 076532. [[CrossRef](#)]
130. Sodeoka, S.; Suzuki, M.; Ueno, K.; Sakuramoto, H.; Shibata, T.; Ando, M. Thermal and mechanical properties of ZrO₂–CeO₂ plasma-sprayed coatings. *J. Therm. Spray Technol.* **1997**, *6*, 361–367. [[CrossRef](#)]
131. Mousavi, B.; Farvizi, M.; Shamsipoor, A.; Rahimipour, M.R.; Keyvani, A. Role of bond coat deposition method on the hot corrosion behavior of CSZ thermal barrier coatings. *Emerg. Mater. Res.* **2023**, *12*, 325–334. [[CrossRef](#)]
132. Keyvani, A.; Bahamirian, M. Hot corrosion and mechanical properties of nanostructured Al₂O₃/CSZ composite TBCs. *Surf. Eng.* **2017**, *33*, 433–443. [[CrossRef](#)]
133. Krogstad, J.A.; Lepple, M.; Levi, C.G. Opportunities for improved TBC durability in the CeO₂–TiO₂–ZrO₂ system. *Surf. Coat. Technol.* **2013**, *221*, 44–52. [[CrossRef](#)]
134. Zinatloo-Ajabshir, S.; Salavati-Niasari, M.; Sobhani, A.; Zinatloo-Ajabshir, Z. Rare earth zirconate nanostructures: Recent development on preparation and photocatalytic applications. *J. Alloys Compd.* **2018**, *767*, 1164–1185. [[CrossRef](#)]
135. Oglezneva, S.A.; Kachenjuk, M.N.; Smetkin, A.A.; Kul'met'eva, V.B. Influence of rare earth elements on the structure and properties of powders based on zirconium dioxide during consolidation. *Int. Conf. Mod. Trends Manuf. Technol. Equip. Mech. Eng. Mater. Sci.* **2020**, *329*, 02015. [[CrossRef](#)]
136. Liu, Z.G.; Zhang, W.H.; Ouyang, J.H.; Zhou, Y. Novel thermal barrier coatings based on rare-earth zirconates/YSZ double-ceramic-layer system deposited by plasma spraying. *J. Alloys Compd.* **2015**, *647*, 438–444. [[CrossRef](#)]
137. Wang, J.D.; Pan, W.; Xu, Q.; Mori, K.; Torigoe, T. Thermal Conductivity of the New Candidate Materials for Thermal Barrier Coatings. *Key Eng. Mater.* **2007**, *280*, 1503–1506. [[CrossRef](#)]
138. Wang, X.; Bai, X.; Xiao, W.; Liu, Y.; Li, X.; Wang, J.; Peng, C.; Wang, L.; Wang, X. Calculation of Thermal Expansion Coefficient of Rare Earth Zirconate System at High Temperature by First Principles. *Materials* **2022**, *15*, 2264. [[CrossRef](#)]
139. Zhou, H.; Yi, D. Effect of rare earth doping on thermo-physical properties of lanthanum zirconate ceramic for thermal barrier coatings. *J. Rare Earths* **2008**, *26*, 770–774. [[CrossRef](#)]
140. Li, F.; Zhou, L.; Liu, J.X.; Liang, Y.; Zhang, G.J. High-entropy pyrochlores with low thermal conductivity for thermal barrier coating materials. *J. Adv. Ceram.* **2019**, *8*, 576–582. [[CrossRef](#)]
141. Liu, D.; Shi, B.; Geng, L.; Wang, Y.; Xu, B.; Chen, Y. High-entropy rare-earth zirconate ceramics with low thermal conductivity for advanced thermal-barrier coatings. *J. Adv. Ceram.* **2022**, *11*, 961–973. [[CrossRef](#)]
142. Wei, Z.Y.; Meng, G.H.; Chen, L.; Li, G.R.; Liu, M.J.; Zhang, W.X.; Zhao, L.N.; Zhang, Q.; Zhang, X.D.; Wan, C.L.; et al. Progress in ceramic materials and structure design toward advanced thermal barrier coatings. *J. Adv. Ceram.* **2022**, *11*, 985–1068. [[CrossRef](#)]
143. Chen, L.; Li, B.; Feng, J. Rare-earth tantalates for next-generation thermal barrier coatings. *Prog. Mater. Sci.* **2024**, *144*, 101265. [[CrossRef](#)]
144. Yang, J.; Qian, X.; Pan, W.; Yang, R.; Li, Z.; Han, Y.; Zhao, M.; Huang, M.; Wan, C. Diffused Lattice Vibration and Ultralow Thermal Conductivity in the Binary Ln–Nb–O Oxide System. *Adv. Mater.* **2019**, *31*, 1808222. [[CrossRef](#)] [[PubMed](#)]
145. Yang, J.; Pan, W.; Han, Y.; Zhao, M.; Huang, M.; Wan, C. Mechanical properties, oxygen barrier property and chemical stability of RE₃NbO₇ for thermal barrier coating. *J. Am. Ceram. Soc.* **2020**, *103*, 2302–2308. [[CrossRef](#)]
146. Wu, F.; Wu, P.; Zhou, Y.; Chong, X.; Feng, J. The thermo-mechanical properties and ferroelastic phase transition of RENbO₄ (RE = Y, La, Nd, Sm, Gd, Dy, Yb) ceramics. *J. Am. Ceram. Soc.* **2020**, *103*, 2727–2740. [[CrossRef](#)]
147. Zhang, P.; Feng, Y.; Li, Y.; Pan, W.; Zong, P.; Huang, M.; Han, Y.; Yang, Z.; Chen, H.; Gong, Q.; et al. Thermal and mechanical properties of ferroelastic RENbO₄ (RE = Nd, Sm, Gd, Dy, Er, Yb) for thermal barrier coatings. *Scr. Mater.* **2020**, *180*, 51–56. [[CrossRef](#)]
148. Chen, L.; Jiang, Y.H.; Chong, X.Y.; Feng, J. Synthesis and thermophysical properties of RETa₃O₉ (RE = Ce, Nd, Sm, Eu, Gd, Dy, Er) as promising thermal barrier coatings. *J. Am. Ceram. Soc.* **2018**, *101*, 1266–1278. [[CrossRef](#)]

149. Chen, L.; Hu, M.; Guo, J.; Chong, X.; Feng, J. Mechanical and thermal properties of RE₂TaO₄ (RE = Yb, Lu, Sc) ceramics with monoclinic-prime phase. *J. Mater. Sci. Technol.* **2020**, *52*, 20–28. [[CrossRef](#)]
150. Majeed, E.A.; Rashid, H.K.; Hussain, M.K. Review of ceramic materials that used as a thermal barrier in diesel engine pistons. *J. Phys. Conf. Ser.* **2021**, *1973*, 012125. [[CrossRef](#)]
151. MatWeb. Mullite. Available online: <https://www.matweb.com/search/DataSheet.aspx?MatGUID=6ff3fda0bf744c93b4e423806faec494> (accessed on 12 March 2024).
152. Xu, H.; Guo, H.; Gong, S. Thermal barrier coatings. In *Developments in High Temperature Corrosion and Protection of Materials*; Woodhead Publishing: Sawston, UK, 2008; pp. 476–491. [[CrossRef](#)]
153. Weinberg, A.V.; Varona, C.; Chaucherie, X.; Goeuriot, D.; Poirier, J. Corrosion of Al₂O₃-SiO₂ refractories by sodium and sulfur vapors: A case study on hazardous waste incinerators. *Ceram. Int.* **2017**, *43*, 5743–5750. [[CrossRef](#)]
154. Syamkumar, K.; Babu, N.; Govindarajan, S.; Arya, S.B. Hot corrosion behaviour of mullite thermal barrier coatings for marine diesel engines. *Ceram. Int.* **2024**, *50*, 2808–2818. [[CrossRef](#)]
155. Chu, K.; Zhang, Y.; Zhao, J.; Liu, Y.; Li, Y.; Li, W.; Liu, B. Screening rare-earth aluminates as promising thermal barrier coatings by high-throughput first-principles calculations. *J. Am. Ceram. Soc.* **2023**, *106*, 3089–3102. [[CrossRef](#)]
156. Torrez-Herrera, J.J.; Fuentes-Ordoñez, E.G.; Ordoñez, E.G.F.; Korili, S.A.; Gil, A. Evidence for the synthesis of La-hexaaluminate from aluminum-containing saline slag wastes: Correction of structural defects and phase purification at low temperature. *Powder Technol.* **2021**, *377*, 80–88. [[CrossRef](#)]
157. Xie, X.; Guo, H.; Gong, S.; Xu, H. Lanthanum–titanium–aluminum oxide: A novel thermal barrier coating material for applications at 1300 °C. *J. Eur. Ceram. Soc.* **2011**, *31*, 1677–1683. [[CrossRef](#)]
158. Zhou, X.; Xu, Z.; Fan, X.; Zhao, S.; Cao, X.; He, L. Y₄Al₂O₉ ceramics as a novel thermal barrier coating material for high-temperature applications. *Mater. Lett.* **2014**, *134*, 146–148. [[CrossRef](#)]
159. Stokes, J.L.; Harder, B.J.; Wiesner, V.L.; Wolfe, D.E. Crystal structures and thermal expansion of Yb₂Si₂O₇–Gd₂Si₂O₇ solid solutions. *J. Solid State Chem.* **2022**, *312*, 123166. [[CrossRef](#)]
160. Guo, L.; Feng, J.; Meng, S. Corrosion resistance of GdPO₄ thermal barrier coating candidate in the presence of CMAS + NaVO₃ and CMAS. *Corros. Sci.* **2022**, *208*, 110628. [[CrossRef](#)]
161. Arshad, M.; Amer, M.; Hayat, Q.; Janik, V.; Zhang, X.; Moradi, M.; Bai, M. High-Entropy Coatings (HEC) for High-Temperature Applications: Materials, Processing, and Properties. *Coatings* **2022**, *12*, 691. [[CrossRef](#)]
162. Patel, P.; Roy, A.; Sharifi, N.; Stoyanov, P.; Chromik, R.R.; Moreau, C. Tribological Performance of High-Entropy Coatings (HECs): A Review. *Materials* **2022**, *15*, 3699. [[CrossRef](#)] [[PubMed](#)]
163. Yao, Y.; Yang, F.; Zhao, X. Multicomponent high-entropy Zr–Y–Yb–Ta–Nb–O oxides for next-generation thermal barrier coating applications. *J. Am. Ceram. Soc.* **2022**, *105*, 35–43. [[CrossRef](#)]
164. Hsu, W.L.; Murakami, H.; Yeh, J.W.; Yeh, A.C.; Shimoda, K. A Heat-Resistant NiCo_{0.6}Fe_{0.2}Cr_{1.5}SiAlTi_{0.2} Overlay Coating for High-Temperature Applications. *J. Electrochem. Soc.* **2016**, *163*, C752. [[CrossRef](#)]
165. Kumar, V.; Kandasubramanian, B. Processing and design methodologies for advanced and novel thermal barrier coatings for engineering applications. *Particuology* **2016**, *27*, 1–28. [[CrossRef](#)]
166. Mehta, A.; Vasudev, H.; Singh, S.; Prakash, C.; Saxena, K.K.; Linul, E.; Buddhi, D.; Xu, J. Processing and Advancements in the Development of Thermal Barrier Coatings: A Review. *Coatings* **2022**, *12*, 1318. [[CrossRef](#)]
167. Latka, L. Thermal Barrier Coatings Manufactured by Suspension Plasma Spraying—A Review. *Adv. Mater. Sci.* **2018**, *18*, 95–117. [[CrossRef](#)]
168. Miranda, F.; Caliarì, F.; Essiptchouk, A.; Pertraconi, G. Atmospheric Plasma Spray Processes: From Micro to Nanostructures. In *Atmospheric Pressure Plasma—From Diagnostics to Applications*; IntechOpen: London, UK, 2019. [[CrossRef](#)]
169. Luo, L.; Chen, Y.; Zhou, M.; Shan, X.; Lu, J.; Zhao, X. Progress update on extending the durability of air plasma sprayed thermal barrier coatings. *Ceram. Int.* **2022**, *48*, 18021–18034. [[CrossRef](#)]
170. Curry, N.; Leitner, M.; Körner, K. High-Porosity Thermal Barrier Coatings from High-Power Plasma Spray Equipment—Processing, Performance and Economics. *Coatings* **2020**, *10*, 957. [[CrossRef](#)]
171. Rabieifar, A.; Mehrizi, V.A.; Haghghi, M.G. Degradation Mechanisms of APS and EB-PVD Thermal Barrier Coatings. *J. Environ. Friendly Mater.* **2023**, *7*, 47–63.
172. Bakan, E.; Mack, D.E.; Mauer, G.; Vaßen, R.; Lamon, J.; Padture, N.P. High-temperature materials for power generation in gas turbines. In *Advanced Ceramics for Energy Conversion and Storage*; Elsevier: Amsterdam, The Netherlands, 2020; pp. 3–62. [[CrossRef](#)]
173. Kubaszek, T.; Goral, M.; Pedrak, P. Influence of air plasma spraying process parameters on the thermal barrier coating deposited with micro- and nanopowders. *Mater. Sci.-Pol.* **2022**, *40*, 80–92. [[CrossRef](#)]
174. Peng, H.; Gong, S. Thermal barrier coatings prepared by electron beam-physical vapor deposition (EB-PVD). In *Thermal Barrier Coatings*, 2nd ed.; Woodhead Publishing: Sawston, UK, 2023; pp. 119–136. [[CrossRef](#)]
175. Lokachari, S.; Leng, K.; Romero, A.R.; Curry, N.; Brewster, G.; Norton, A.; Hussain, T. Processing–Microstructure–Properties of Columns in Thermal Barrier Coatings: A Study of Thermo-Chemico-Mechanical Durability. *ACS Appl. Mater. Interfaces* **2024**, *16*, 10646–10660. [[CrossRef](#)] [[PubMed](#)]
176. Iqbal, A.A.; Lim, M.J. A relationship of porosity and mechanical properties of spark plasma sintered scandia stabilized zirconia thermal barrier coating. *Results Eng.* **2023**, *19*, 101263. [[CrossRef](#)]

177. Curry, N.; VanEvery, K.; Snyder, T.; Markocsan, N. Thermal Conductivity Analysis and Lifetime Testing of Suspension Plasma-Sprayed Thermal Barrier Coatings. *Coatings* **2014**, *4*, 630–650. [[CrossRef](#)]
178. Yamazaki, Y.; Morikawa, M.; Hamaguchi, T.; Habu, Y.; Ohide, Y.; Takagi, K. Relationship between the mechanical properties and structure of a suspension plasma-sprayed thermal barrier coating with columnar microstructure. *Surf. Coat. Technol.* **2022**, *439*, 128430. [[CrossRef](#)]
179. Tesar, T.; Musalek, R.; Medricky, J.; Cizek, J. On growth of suspension plasma-sprayed coatings deposited by high-enthalpy plasma torch. *Surf. Coat. Technol.* **2019**, *371*, 333–343. [[CrossRef](#)]
180. Bernard, B.T.; Quet, A.; Bianchi, L.; Schick, V.; Joulia, A.; Malié, A.; Rémy, B. Effect of Suspension Plasma-Sprayed YSZ Columnar Microstructure and Bond Coat Surface Preparation on Thermal Barrier Coating Properties. *J. Therm. Spray Technol.* **2017**, *26*, 1025–1037. [[CrossRef](#)]
181. Gao, Y.; Zhao, Y.; Yang, D.; Gao, J. A Novel Plasma-Sprayed Nanostructured Coating with Agglomerated-Unsintered Feedstock. *J. Therm. Spray Technol.* **2016**, *25*, 291–300. [[CrossRef](#)]
182. Zhu, J.; Ma, K. Microstructural and mechanical properties of thermal barrier coating at 1400 °C treatment. *Theor. Appl. Mech. Lett.* **2014**, *4*, 021008. [[CrossRef](#)]
183. Dwivedi, G.; Viswanathan, V.; Sampath, S.; Shyam, A.; Lara-Curzio, E. Fracture toughness of plasma sprayed thermal barrier ceramics: Influence of processing, microstructure, and thermal aging. *J. Am. Ceram. Soc.* **2014**, *97*, 2736–2744. [[CrossRef](#)]
184. Mahade, S.; Venkat, A.; Curry, N.; Leitner, M.; Joshi, S. Erosion Performance of Atmospheric Plasma Sprayed Thermal Barrier Coatings with Diverse Porosity Levels. *Coatings* **2021**, *11*, 86. [[CrossRef](#)]
185. Boissonnet, G.; Bonnet, G.; Pasquet, A.; Bourhila, N.; Pedraza, F. Evolution of thermal insulation of plasma-sprayed thermal barrier coating systems with exposure to high temperature. *J. Eur. Ceram. Soc.* **2019**, *39*, 2111–2121. [[CrossRef](#)]
186. Hu, Z.C.; Liu, B.; Wang, L.; Cui, Y.H.; Wang, Y.W.; Ma, Y.D.; Sun, W.W.; Yang, Y. Research Progress of Failure Mechanism of Thermal Barrier Coatings at High Temperature via Finite Element Method. *Coatings* **2020**, *10*, 732. [[CrossRef](#)]
187. Liu, G.; Shen, Z.; He, L.; Mu, R.; Huang, G. LaYZrO/YSZ double ceramic layer thermal barrier coatings by EB-PVD: Thermal performance, morphology and failure behavior. *Materialia* **2023**, *27*, 101661. [[CrossRef](#)]
188. Mahade, S.; Li, R.; Curry, N.; Björklund, S.; Markocsan, N.; Nylén, P. Isothermal Oxidation Behavior of Gd₂Zr₂O₇/YSZ Multilayered Thermal Barrier Coatings. *Int. J. Appl. Ceram. Technol.* **2016**, *13*, 443–450. [[CrossRef](#)]
189. Mahade, S.; Curry, N.; Björklund, S.; Markocsan, N.; Joshi, S. Durability of Gadolinium Zirconate/YSZ Double-Layered Thermal Barrier Coatings under Different Thermal Cyclic Test Conditions. *Materials* **2019**, *12*, 2238. [[CrossRef](#)]
190. Mondal, K.; Nunez, L.; Downey, C.M.; van Rooyen, I.J. Thermal Barrier Coatings Overview: Design, Manufacturing, and Applications in High-Temperature Industries. *Ind. Eng. Chem. Res.* **2021**, *60*, 6061–6077. [[CrossRef](#)]
191. Sathish, M.; Radhika, N.; Saleh, B. A critical review on functionally graded coatings: Methods, properties, and challenges. *Compos. Part B Eng.* **2021**, *225*, 109278. [[CrossRef](#)]
192. Bhavar, V.; Kattire, P.; Thakare, S.; Patil, S.; Singh, R.K.P. A Review on Functionally Gradient Materials (FGMs) and Their Applications. *IOP Conf. Ser. Mater. Sci. Eng.* **2017**, *229*, 012021. [[CrossRef](#)]
193. Kagerer, S.; Hudak, O.E.; Schloffer, M.; Riedl, H.; Mayrhofer, P.H. TGO formation and oxygen diffusion in Al-rich gamma-TiAl PVD-coatings on TNM alloys. *Scr. Mater.* **2022**, *210*, 114455. [[CrossRef](#)]
194. Ding, K.; Zhang, T.; Wang, Z.; Yu, J.; Guo, W.; Yang, Y. Effect of Thermal Growth Oxide Composition and Morphology on Local Stresses in Thermal Barrier Coatings. *Materials* **2022**, *15*, 8442. [[CrossRef](#)] [[PubMed](#)]
195. Osorio, J.D.; Toro, A.; Hernández-Ortiz, J.P. Thermal Barrier Coatings for Gas Turbine Applications: Failure Mechanisms and Key Microstructural Features. *Dyna* **2012**, *79*, 149–158.
196. Dong, H.; Yang, G.J.; Li, C.X.; Luo, X.T.; Li, C.J. Effect of TGO Thickness on Thermal Cyclic Lifetime and Failure Mode of Plasma-Sprayed TBCs. *J. Am. Ceram. Soc.* **2014**, *97*, 1226–1232. [[CrossRef](#)]
197. Ding, H.; Dong, H.; Li, C.J.; Yang, G.J. Effect of TGO Thickness on Isothermal Cyclic Lifetime of Plasma-Sprayed YSZ Thermal Barrier Coatings. In Proceedings of the International Thermal Spray Conference, Long Beach, CA, USA, 11–14 May 2015; pp. 801–805. [[CrossRef](#)]
198. Torkashvand, K.; Poursaeidi, E.; Mohammadi, M. Effect of TGO thickness on the thermal barrier coatings life under thermal shock and thermal cycle loading. *Ceram. Int.* **2018**, *44*, 9283–9293. [[CrossRef](#)]
199. Evans, A.G.; Hutchinson, J.W. On the mechanics of delamination and spalling in compressed films. *Int. J. Solids Struct.* **1984**, *20*, 455–466. [[CrossRef](#)]
200. Bhatnagar, H.; Ghosh, S.; Walter, M.E. Parametric studies of failure mechanisms in elastic EB-PVD thermal barrier coatings using FEM. *Int. J. Solids Struct.* **2006**, *43*, 4384–4406. [[CrossRef](#)]
201. Wei, Z.Y.; Cai, H.N. Comprehensive effects of TGO growth on the stress characteristic and delamination mechanism in lamellar structured thermal barrier coatings. *Ceram. Int.* **2020**, *46*, 2220–2237. [[CrossRef](#)]
202. Yuan, B.; Harvey, C.M.; Thomson, R.C.; Critchlow, G.W.; Rickerby, D.; Wang, S. A new spallation mechanism of thermal barrier coatings and a generalized mechanical model. *Compos. Struct.* **2019**, *227*, 111314. [[CrossRef](#)]
203. Eriksson, R. Thermal Barrier Coatings—Durability Assessment and Life Prediction. Doctoral Dissertation, Linköping University, Linköping, Sweden, 2013. ISSN 0345-7524.
204. Evans, A.G.; He, M.Y.; Hutchinson, J.W. Mechanics-based scaling laws for the durability of thermal barrier coatings. *Prog. Mater. Sci.* **2001**, *46*, 249–271. [[CrossRef](#)]

205. Renusch, D.P.; Rudolphi, M.; Schütze, M. Software Tools for Lifetime Assessment of Thermal Barrier Coatings Part II—Bond Coat Aluminum Depletion Failure. *J. Solid Mech. Mater. Eng.* **2010**, *4*, 155–166. [CrossRef]
206. Shillington, E.A.G.; Clarke, D.R. Spalling failure of a thermal barrier coating associated with aluminum depletion in the bond-coat. *Acta Mater.* **1999**, *47*, 1297–1305. [CrossRef]
207. Jonnalagadda, K.P. Thermal Barrier Coatings Failure Mechanisms and Life Prediction. Doctoral Thesis, Linköping University, Linköping, Sweden, 2019. ISSN 0345-7524.
208. Lim, L.Y.; Meguid, S.A. Modeling and characterisation of depletion of aluminium in bond coat and growth of mixed oxides in thermal barrier coatings. *Int. J. Mech. Mater. Des.* **2020**, *16*, 667–683. [CrossRef]
209. Taylor, M.; Evans, H.E.; Gray, S.; Nicholls, J.R. A chromia forming thermal barrier coating system. *Mater. Corros.* **2011**, *62*, 668–673. [CrossRef]
210. Berthod, P. Kinetics of High Temperature Oxidation and Chromia Volatilization for a Binary Ni–Cr Alloy. *Oxid. Met.* **2005**, *64*, 235–252. [CrossRef]
211. Eriksson, R. High-Temperature Degradation of Plasma Sprayed Thermal Barrier Coating Systems. Doctoral Thesis, Linköping University, Linköping, Sweden, 2011. ISSN 0280-7971.
212. Wang, L.; Zhao, Y.X.; Zhong, X.H.; Tao, S.Y.; Zhang, W.; Wang, Y. Influence of “Island-Like” Oxides in the Bond-Coat on the Stress and Failure Patterns of the Thermal-Barrier Coatings Fabricated by Atmospheric Plasma Spraying During Long-Term High Temperature Oxidation. *J. Therm. Spray Technol.* **2014**, *23*, 431–446. [CrossRef]
213. Zou, Z.; Jia, L.; Yang, L.; Shan, X.; Luo, L.; Guo, F.; Zhao, X.; Xiao, P. Role of internal oxidation on the failure of air plasma sprayed thermal barrier coatings with a double-layered bond coat. *Surf. Coat. Technol.* **2017**, *319*, 370–377. [CrossRef]
214. Sun, X.; Zhang, P.; Moverare, J.; Li, X.H.; Cui, L.; Peng, R.L. Impeding the γ' depletion during the interdiffusion between bond coatings and superalloys via introduction of tantalum in bond coatings. *Mater. Des.* **2023**, *227*, 111792. [CrossRef]
215. Liu, Y.; Yin, B.; Deng, C.; Li, Q.; Zhang, L.; Deng, P.; Yang, K.; Wu, C.; Liu, M. Microstructure evolution and interdiffusion behaviors of (Ni,Pt)Al coating with and without Re-diffusion barrier on IC21 substrate at 1100 °C. *Mater. Charact.* **2021**, *181*, 111450. [CrossRef]
216. Rouzou, L.; Molins, R.; Rémy, L.; Jomard, F. Study of the Sulfur Segregation for a TBC System. *Mater. Sci. Forum* **2004**, *461–464*, 101–108. [CrossRef]
217. Bai, M.; Jiang, H.; Chen, Y.; Chen, Y.; Grovenor, C.; Zhao, X.; Xiao, P. Migration of sulphur in thermal barrier coatings during heat treatment. *Mater. Des.* **2016**, *97*, 364–371. [CrossRef]
218. Bacos, M.P.; Dorvaux, J.M.; Lavigne, O.; Mévrel, R.; Poulain, M.; Rio, C.; Vidal-Sétif, M.H. Performance and Degradation Mechanisms of Thermal Barrier Coatings for Turbine Blades: A Review of ONERA Activities. *Aerosp. Lab* **2011**, *3*, 1–11.
219. Hou, P.Y. Segregation Behavior at TGO/Bondcoat Interfaces. *J. Mater. Sci.* **2009**, *44*, 1711–1725. [CrossRef]
220. Smialek, J.L.; Pint, B.A. Optimizing Scale Adhesion on Single Crystal Superalloys. *Mater. Sci. Forum* **2001**, *369–372*, 459–466. [CrossRef]
221. Faucett, D.C.; Wright, J.; Ayre, M.; Choi, S.R. Foreign Object Damage (FOD) in Thermal Barrier Coatings. *Ceram. Trans.* **2012**, *234*, 245–255. [CrossRef]
222. Wannman, C. Erosion Behaviour of Thermal Barrier Coatings. Master’s Thesis, Linköping University, Linköping, Sweden, 2021.
223. Yu, X.; Li, C.; Chang, S.; Xuan, C.; Peiyuan, L. Foreign Object Damage Performance and Constitutive Modeling of Titanium Alloy Blade. *Int. J. Aerosp. Eng.* **2020**, *2020*, 2739131. [CrossRef]
224. Wellman, R.G.; Deakin, M.J.; Nicholls, J.R. The effect of TBC morphology on the erosion rate of EB PVD TBCs. *Wear* **2005**, *258*, 349–356. [CrossRef]
225. Nicholls, J.R.; Wellman, R.G. Erosion and Foreign Object Damage of Thermal Barrier Coatings. *Mater. Sci. Forum* **1997**, *251–254*, 935–948. [CrossRef]
226. Chen, X.; Hutchinson, J.W. Particle impact on metal substrates with application to foreign object damage to aircraft engines. *J. Mech. Phys. Solids* **2002**, *50*, 2669–2690. [CrossRef]
227. Chen, X.; Wang, R.; Yao, N.; Evans, A.G.; Hutchinson, J.W.; Bruce, R.W. Foreign object damage in a thermal barrier system: Mechanisms and simulations. *Mater. Sci. Eng. A* **2003**, *352*, 221–231. [CrossRef]
228. Pettit, F. Hot Corrosion of Metals and Alloys. *Oxid. Met.* **2011**, *76*, 1–21. [CrossRef]
229. Carlsson, K. A Study of Failure Development in Thick Thermal Barrier Coatings. Master’s Thesis, Linköping University, Linköping, Sweden, 2007.
230. Holländer, C.; Kiliani, S.; Stamm, W.; Lüsebrink, O.; Harders, H.; Wessel, E.; Müller, M.; Singheiser, L. Hot corrosion of TBC-coated components upon combustion of low-sulfur fuels. *Mater. Corros.* **2021**, *72*, 1643–1655. [CrossRef]
231. Ozgurluk, Y.; Doleker, K.M.; Ahlatci, H.; Karaoglanli, A.C. Investigation of hot corrosion behavior of thermal barrier coating (TBC) systems with rare earth contents. *Arab. J. Geosci.* **2018**, *11*, 267. [CrossRef]
232. National Center for Biotechnology Information. PubChem Compound Summary for CID 24436, Sodium Sulfate. Available online: <https://pubchem.ncbi.nlm.nih.gov/compound/Sodium-Sulfate> (accessed on 20 February 2024).
233. National Center for Biotechnology Information. PubChem Compound Summary for CID 5234, Sodium Chloride. Available online: <https://pubchem.ncbi.nlm.nih.gov/compound/Sodium-Chloride> (accessed on 20 February 2024).
234. National Center for Biotechnology Information. PubChem Compound Summary for CID 14814, Vanadium Pentoxide. Available online: <https://pubchem.ncbi.nlm.nih.gov/compound/Vanadium-pentoxide> (accessed on 20 February 2024).

235. Morelli, S.; Bursich, S.; Testa, V.; Bolelli, G.; Miccichè, A.; Lusvarghi, L. CMAS corrosion and thermal cycling fatigue resistance of alternative thermal barrier coating materials and architectures: A comparative evaluation. *Surf. Coat. Technol.* **2022**, *439*, 128433. [[CrossRef](#)]
236. Meng, F.; Ye, F.; Luo, T. The high-temperature CMAS corrosion behavior of high-entropy $(\text{La}_{0.2}\text{Nd}_{0.2}\text{Sm}_{0.2}\text{Eu}_{0.2}\text{Gd}_{0.2})_2\text{Hf}_2\text{O}_7$ hafnate thermal barrier coating material with fluorite structure. *J. Eur. Ceram. Soc.* **2024**, *44*, 2460–2470. [[CrossRef](#)]
237. Mahade, S. Functional Performance of Gadolinium Zirconate/Yttria Stabilized Zirconia Multi-Layered Thermal Barrier Coatings. Doctoral Thesis, University West, Trollhättan, Sweden, 2018. ISBN 978-91-87531-85-9.
238. Li, D.; Jiang, P.; Gao, R.; Sun, F.; Jin, X.; Fan, X. Experimental and numerical investigation on the thermal and mechanical behaviours of thermal barrier coatings exposed to CMAS corrosion. *J. Adv. Ceram.* **2021**, *10*, 551–564. [[CrossRef](#)]
239. Levi, C.G.; Hutchinson, J.W.; Vidal-Sétif, M.H.; Johnson, C.A. Environmental degradation of thermal-barrier coatings by molten deposits. *MRS Bull.* **2012**, *37*, 932–941. [[CrossRef](#)]
240. Yan, J.; Wang, X.; Chen, K.; Lee, K.N. Sintering Modeling of Thermal Barrier Coatings at Elevated Temperatures: A Review of Recent Advances. *Coatings* **2021**, *11*, 1214. [[CrossRef](#)]
241. Aygun, A. Novel Thermal Barrier Coatings (TBCs) That Are Resistant to High Temperature Attack by CaO-MgO-Al₂O₃-SiO₂ (CMAS) Glassy Deposits. Doctoral Thesis, The Ohio State University, Columbus, OH, USA, 2008.
242. Wellman, R.G.; Nicholls, J.R. Erosion, corrosion and erosion–corrosion of EB PVD thermal barrier coatings. *Tribol. Int.* **2008**, *41*, 657–662. [[CrossRef](#)]
243. Wang, L.S.; Song, J.B.; Dong, H.; Yao, J.T. Sintering-Induced Failure Mechanism of Thermal Barrier Coatings and Sintering-Resistant Design. *Coatings* **2022**, *12*, 1083. [[CrossRef](#)]
244. Tian, H.; Wei, L.; He, L. Phase Composition and Stability, Sintering and Thermal Conductivity of Gd₂O₃ and Yb₂O₃ Co-Doped YSZ. *Coatings* **2023**, *13*, 53. [[CrossRef](#)]
245. Yi, H.; Che, J.; Liang, G.; Liu, X. Effect of Rare Earth Elements on Stability and Sintering Resistance of Tetragonal Zirconia for Advanced Thermal Barrier Coatings. *Crystals* **2021**, *11*, 287. [[CrossRef](#)]
246. Ali, M.Y.; Nusier, S.Q.; Newaz, G.M. Creep effects on early damage initiation in a TBC system. *J. Mater. Sci.* **2004**, *39*, 3383–3390. [[CrossRef](#)]
247. Gupta, C.K. Nuclear Reactor Materials. In *Encyclopedia of Materials: Science and Technology*, 2nd ed.; Elsevier: Amsterdam, The Netherlands, 2001; pp. 6339–6349. [[CrossRef](#)]
248. Scott MacKenzie, D. The mechanism of creep and its stages. In *Thermal Processing. Hot Seat*; Thermal Processing: Yeager Parkway Pelham, AL, USA, 2024; pp. 24–25.
249. Pelleg, J. *Creep in Ceramics*; Springer: Berlin/Heidelberg, Germany, 2017; Volume 241, pp. 41–61. [[CrossRef](#)]
250. Schmidt, U.T.; Vohringer, O.; Lohe, D. The Creep Damage Behavior of the Plasma-Sprayed Thermal Barrier Coating System NiCr₂₂Co₁₂Mo₉-NiCoCrAlY-ZrO₂/7%Y₂O₃. *J. Eng. Gas Turbines Power* **1999**, *121*, 678–682. [[CrossRef](#)]
251. Yang, L.; Zou, Z.; Kou, Z.; Chen, Y.; Zhao, G.; Zhao, X.; Guo, F.; Xiao, P. High temperature stress and its influence on surface rumpling in NiCoCrAlY bond coat. *Acta Mater.* **2017**, *139*, 122–137. [[CrossRef](#)]
252. Xu, B.Q.; Luo, L.R.; Lu, J.; Zhao, X.F.; Xiao, P. Effect of residual stress on the spallation of the thermally-grown oxide formed on NiCoCrAlY coating. *Surf. Coat. Technol.* **2020**, *381*, 125112. [[CrossRef](#)]
253. Panat, R.; Zhang, S.; Hsia, K.J. Bond coat surface rumpling in thermal barrier coatings. *Acta Mater.* **2003**, *51*, 239–249. [[CrossRef](#)]
254. Mahfouz, L.; Marchand, B.; Guipont, V.; Coudon, F.; Maurel, V. Driving forces in thermal barrier coatings blistering. *Materialia* **2023**, *28*, 101728. [[CrossRef](#)]
255. Chen, Y.; Zhao, X.; Bai, M.; Yang, L.; Li, C.; Wang, L.; Carr, J.A.; Xiao, P. A mechanistic understanding on rumpling of a NiCoCrAlY bond coat for thermal barrier coating applications. *Acta Mater.* **2017**, *128*, 31–42. [[CrossRef](#)]

Disclaimer/Publisher’s Note: The statements, opinions and data contained in all publications are solely those of the individual author(s) and contributor(s) and not of MDPI and/or the editor(s). MDPI and/or the editor(s) disclaim responsibility for any injury to people or property resulting from any ideas, methods, instructions or products referred to in the content.